Impact of well-watered trees on the microclimate inside a canyon street scale model in outdoor environment

S. Mballo, S. Herpin, M. Manteau, Sabine Demotes-Mainard, P.E. Bournet

Impact of well-watered trees on the microclimate inside a canyon street scale model in outdoor environment

S. Mballo[1,*], S. Herpin[1,2], M. Manteau[1,2], S. Demotes-Mainard[3] and P.E. Bournet[1,2]

[1]*EPHor, Institut Agro, SFR 4207 QuaSaV, 49045 Angers, France*

[2]*IRSTV, FR CNRS 2488, 44321 Nantes Cedex 3, France*

[3]*Univ Angers, Institut Agro, INRAE, IRHS, SFR QUASAV, F-49000 Angers, France*

[*]*souleymane.mballo@agrocampus-ouest.fr*

Abstract – Cities experience overheating due to factors such as urban form and materials, concentration of human activities, reduction in the amount of vegetation and water surfaces. Vegetation is one of the ways to reduce temperature peaks in the city during heat waves. The objectives of this paper are twofold: first, to study the impact on the microclimate of a north-south oriented canyon street at reduced-scale (1/5), then to study the impact of well-watered trees on the street microclimate. This study provides a highly integrated view of climatic mechanisms through the measurement of a set variables, including air temperature, relative humidity, wall temperature, conductive and radiation fluxes as well as tree transpiration and thus allows a better understanding of the physical phenomena at stake. It shows that the canyon street created an urban overheating of up to 2.8 °C during the night, and up to 2.4 °C during the day, and that trees reduced the air temperature in the street by up to 2.7 °C during the day. Finally, trees improved human thermal comfort with a reduction of 8 °C of the Universal Thermal Climate Index at midday.

Keywords: Energy balance, Radiation, water balance, transpiration, thermal comfort, urban environment

1 Introduction

Urbanization is the process of migration of people from rural area to urban area for the improvement of their lives (Kuddus and Rahman, 2015). At the beginning of the twentieth century, 15 % of the world population lived in cities (Susca et al., 2011). In 2018, 55 % of the world's population resided in urban areas, and by 2050, 68 % of the world's population is projected to be urban (United Nations, 2018). In Europe, the urbanization rate was already 74.5 % in 2018 and a projection indicates that this rate will reach 83.7 % in 2050 (United Nations, 2018). The trend towards urbanization leads to the expansion of cities and the replacement of vegetation, natural soil, and water surface by impervious surfaces such as asphalt. The effect of urbanization on the urban thermal environment has attracted increasing research attention for its significant relationship to local climatic change and habitat comfort (Xiong et al., 2012). Among the consequences of urbanization on the urban microclimate is the Urban Heat Island (UHI) phenomenon, which is a heat accumulation process within an urban area due to urban buildings and human activities (Yang et al., 2016). According to Rizwan et al. (2008), UHI is one of the biggest environmental problems of the 21st century caused by the urbanization and industrialization of our society. Extensive studies of the characteristics of UHI effect were carried out in recent decades by authors such as Aboelata (2020); Arnfield (2003); Cantat (2004); Chen et al. (2006); Ridha (2017); Rizwan et al. (2008); Santamouris et al. (2001); Weng et al. (2004) and Yang et al. (2016). They showed that the UHI effects (in terms of intensity in particular) vary from one place to another as they are closely related to urban heat release, surface properties, vegetation coverage, population density. Measured air temperature in UHI can exceed 10 °C compared with the neighboring rural areas for the city of Athens (Santamouris et al., 2001) and 11.4 °C in Paris (Cantat, 2004).

Among the different existing urban topologies, canyon streets are a classical downtown configuration and therefore deserve a particular attention. A canyon street is a straight street continuously bordered by tall buildings. Since the pioneering work of Oke (1988), canyon streets are an emblematic configuration

of urban microclimate research on which many data are available. They are generally defined by their aspect ratio which is the ratio between the height of the buildings and the width of the street (or the inverse depending on the authors) and the orientation of their main axis. Canyon streets are ideal places to observe different phenomena at stake in the UHI such as wind sheltering effect (when the wind blows perpendicularly to the street), and radiative trapping (resulting from absorption and reflection of solar radiation during daytime, and retention of long-wave radiation at night). They are also often considered as a geometry of reference in modelling tools. The TEB (Town Energy Budget) model for instance is able to simulate the climate of an entire city from the prediction of the climate inside a set of canyon streets (Lemonsu et al., 2004; Redon, 2017; Redon et al., 2020). Many outdoor experimental studies on canyon street focused on aeraulics and turbulence phenomena (Andreou, 2014; DePaul and Sheih, 1986, 1986; Georgakis and Santamouris, 2006; Louka et al., 2002; Najjar et al., 2005; Nakamura and Oke, 1988; Niachou et al., 2008; Rotach, 1995; Rotach et al., 2005) and will not be further commented here. In the following, we will focus our attention on studies dedicated to urban microclimate inside canyon streets, including thermal effects, without (Table 1) or with (Table 2) vegetation.

We have listed in Table 1 the main studies carried out on non-vegetated urban full-scale or reduced-scale canyon streets. The aspect ratio in this table is calculated as the ratio of building height to street width. The scales for the reduced-scale canyon streets are determined from a reference height of 10 m. Table 1 shows that prior to the 2000s, experimental studies on canyon streets were essentially full-scale. Indeed, full-scale outdoor experimental studies make it possible to assess several physical phenomena at the same time with fewer hypotheses. In particular for full-scale studies, Najjar et al. (2005) studied a canyon street in Strasbourg Eastern France oriented north north-east/south south-west with an aspect ratio of 0.9. The experiment was focused on the radiation balance of the street, but also looked at sensible and latent heat flux. Many authors have also been interested in the impact of canyon street orientation on the microclimate (Andreou, 2014; Eliasson, 1996). They have found that for the same aspect ratio, the interception of solar radiation by the solid walls, and thus the wall and air temperatures, depended on both the orientation of the street and the inclination of the sun. Andreou (2014) showed, for example, that the ground of north-south oriented streets, in comparison to east-west oriented streets, is more shaded during summertime, and less shaded during wintertime. As for the wall façades, north-south oriented streets receive more solar radiation than east-west oriented streets in summer. This was observed for aspect ratios within the range [0.6; 3]. The author also showed that the larger the aspect ratio, the more important the shading in the street, especially for North-South oriented streets.

However, more and more outdoor canyon street experimental studies now tend to be conducted at a reduced-scale despite the difficulties associated with the transposition of results to full-scale. To our knowledge, there are for the moment only 4 models of purely mineral canyon streets that have been built outdoors at reduced-scale, with scale reduction factor ranging from 1/2 to 1/8. Athamena et al. (2018) studied a reduced-scale (1/2) canyon street in an outdoor environment in Nantes, looking at phenomena coupling aeraulics and thermics. Idczak et al. (2007) conducted micrometeorological measurements at an experimental site (scale 1/2) located in the industrial area of Guerville (48°56’N, 1°44’W) in France. Idczak et al. (2007) observed that thermal effects were significant only in areas close to walls, and that buoyancy forces were generally negligible in the canyon street. Wang et al. (2017) carried out field experiments in an east-west 1/8 scale canyon street built in Sun Yat-Sen University, Guangzhou, China (23°4’N, 113°23’E) to study the impact of thermal mass of walls on air and wall temperatures. Their measurements show that during the daytime, walls with the lowest thermal mass reach their peaks earlier than walls with the highest thermal mass and that the opposite results occur after sunset. Chen et al. (2020) used the same experimental facility with various aspect ratios of the streets. Their studies showed that thermal storage capacity and aspect ratio are two essential factors that determine the urban

microclimate. On the aspect ratio, they found that the wider the street, i.e., the lower the ratio between the height of the buildings and the width of the street, the higher the wall and air temperatures during daytime. On the contrary, during the night, the street with lower aspect ratio cools down faster.

As far as urban vegetation is concerned, Bowler et al. (2010) and Jamei et al. (2016) conducted a state-of-the-art review on studies focusing on the effect of green spaces on temperature and thermal comfort. Bowler et al. (2010) found that authors were more interested in the effect of parks and trees than in the effect of green roofs. All studies with urban green spaces show that they have an impact on the environment, at least locally. In canyon streets, trees can have cooling or warming effects on the air depending on their position on the street, prevailing wind conditions and time of day. During the day, the effects of trees are more noticeable in shallow streets because, in deep streets, their effects are masked by buildings (Bowler et al., 2010; Jamei et al., 2016). During the night, the air temperature beneath trees in deep canyons is slightly higher than the surrounding air temperature due to the low sky view factor that blocks infrared cooling (Jamei et al., 2016). In Table 2, we have listed studies dedicated to vegetation inside canyon streets, both at full-scale and reduced-scale. As it can be seen, most studies were conducted in temperate climate, as already pointed out by Bowler et al. (2010). In spite of the diversity of tree species used, it can be seen that trees organized in two lateral rows is the most frequently considered configuration. Table 2 also shows that information about vegetation such as LAI (Leaf Area Index, defined as the ratio of the cumulated leaf surfaces to the projected area of the crown to the ground), LAD (Leaf Area Density, defined as the ratio of cumulated leaf surfaces to crown volume) and part of ground covered vegetation vary from one study to another. Therefore, configurations are often not easy to compare to one another, and a very broad range of air temperature reduction by trees (from 0.4°C to 6°C) has been reported in the literature, depending on the authors. To date, most of the studies on the impact of vegetation on the microclimate in a canyon street have been carried out at full-scale. In Dresden, Gillner et al. (2015) showed that, thanks to the shading effects, vegetation can reduce surface temperatures by 5.5 to 15.2 °C and air temperature by 0.7 to 2.2 K depending on the tree species used. The authors also showed that trees can reduce asphalt temperatures by up to 4.6 °C per unit of LAD Gebert et al. (2019) are some of the few authors to have measured the water content by volume in soil. Their results showed that stomatal conductance (and thus tree transpiration) was closely related to soil water availability. On the impact of trees on human thermal comfort, Coutts et al. (2016) found that, during heat events, trees in East-West oriented Canyons with average aspect ratio comprised between 0.27 and 0.76 had a low impact on air temperature (0.9 °C at mid-morning) but a significant impact on diurnal index in summer, largely due to a reduction in the mean radiant temperature, reducing heat stress from a very high level (UTCI > 38°C) to a high level (38 °C > UTCI > 32 °C). We found only three studies in the literature (Djedjig et al., 2013, Ouldboukhitine et al., 2011; Park et al., 2012) that were conducted in reduced-scale street. The first two studies focused only on green walls and roofs and Park et al. (2012) were the only ones to consider trees in their street. Park et al. (2012) conducted a study in Japan (39°04', 139°07'E) on a small-scale (1/10) urban model on the effect of urban vegetation on the outdoor thermal environment. They found that trees, in comparison with a non-vegetated modality, could reduce the globe temperature (which incorporates the effects of radiation, so this magnitude is different from the air temperature) by 0.6 to 2.2 °C depending on the street orientation and sensors position.

In this paper, we propose to study the impact of a canyon street on the microclimate, and then to study the impact of trees on the microclimate within the canyon street. To reach this goal, we first present the 1/5 scale canyon used for experiments, the instrumentation, and the method of calculation of several quantities of interest. Second, in addition to the variables classically studied in the literature such as air temperatures, wall temperatures, relative and absolute humidities, we analyze other variables such as tree

136 transpiration, radiation and its interception by buildings and trees both in areas without or with trees. An
137 originality of the present study also relies on the fact that the soil was instrumented, which gave access
138 to the soil water status, whereas this information is very rarely available in urban studies. We also
139 investigate the thermal comfort inside the street in the vegetated and non-vegetated modalities and
140 compare it to a control rural-like environment outside the street. A discussion including considerations
141 on the representativeness of the reduced-scale street and on the limitations and perspectives of the present
142 work is also provided.

References	Place	Köppen-Geiger climate type	Orientation	Model	Scale	Aspect ratio (H/W)	Measured variables[1]
Chen et al. (2020)	Guangzhou, China	Cwa, Cfa	E-W	Reduced	1/8	1.0, 2.0, 3.0	WS, AT, ST, SHF, RAD
Athamena et al. (2018)	Nantes, France	Cfb	NE-SW	Reduced	1/2	1.4	WS, AT
Liang et al. (2018)	Guangzhou, China	Cwa, Cfa	NW-SE	Reduced	1/8	1.0, 2.0, 3.0	WS, AT
Wang et al. (2017)	Guangzhou, China	Cwa, Cfa	E-W	Reduced	1/8	1.0	WS, AT, ST, HF, RAD
Andreou (2014)	Island of Tinos, Greece	Csa	Many	Full	-	2.0, 0.7, 0.9	WS, AT, ST, RAD
Doya et al. (2012)	La Rochelle, France	Cfb	N-S	Reduced	1/8	1.1	AT, ST
Niachou et al. (2008)	Athens, Greece	Csa	ESE-WNW	Full	-	1.7	WS, AT, ST
Idczak et al. (2007)	Guerville, France	Cfb	NE-SW	Reduced	1/2	2.2	WS, AT, ST, HF, RAD
Georgakis and Santamouris (2006)	Athens, Greece	Csa	NW-SE	Full	-	3.3	WS, AT, ST
Najjar et al. (2005)	Strasbourg, France	Cfb	NNE-SSW	Full	-	0.9	SHF, LHF, RAD
Rotach et al. (2005)	Basel, Switzerland	Cfb	-	Full	-	-	WS, AT, SHF, LHF, RAD
Bourbia and Awbi (2004)	El-Oued, Algeria	BWh	E-W, N-S	Full	-	1.3, 4.0, 2.0	AT, ST
Louka et al. (2002)	Nantes, France	Cfb	N-S	Full	-	1.4	WS, AT, ST
Santamouris et al. (1999)	Athens, Greece	Csa	NW-SE	Full	-	2.5	WS, AT, ST
Eliasson (1996)	Göteborg, Sweden	Dfb	ENE-WSW, NNW-SSE	Full	-	1.4-2.1	AT, ST
Nakamura and Oke (1988)	Kyoto, Japan	Cfa	E-W	Full	-	1.0	WS, AT, ST
DePaul and Sheih (1986)	Chicago, USA	Dfa	N-S	Full	-	1.4	WS

Table 1: Main studies carried out on canyon streets in outdoor environment. The scale of the street in a reduced environment is determined in relation to a reference height of 10 m. The orientation refers to the direction of the main axis of the street. Variable names are AT: Air Temperature, Emax: Evapotranspiration maximum, Gs: Stomatal conductance, HF: Heat Flux, LHF: Latent Heat Flux, LT: Leaf Temperature, RAD: Radiation, RH: Relative Humidity, SHF: Sensible Heat Flux, ST: Surface Temperature, UTCI: Universal Thermal Climate Index, WS: Wind Speed. Climate characteristics refer to the Köppen-Geiger classification**:** BWk: Semi-arid climate, BWh: Arid climate, Cfa: Humid subtropical climates, Cfb: Oceanic climate, Csa: Mediterranean hot summer climates, Cwa: Dry-winter humid, subtropical climate, Dfa: Hot summer continental climates, Dfb: Warm summer continental or hemiboreal climates**.**

References	Place	Köppen-Geiger	Orientation	Model	Scale	H/W	Type of vegetation	Other information about vegetation[2]	Measured or calculated variables[3]
Aboelata (2020)	Cairo, Egypt	BWh	NW-SE	Full	-	1.0	Trees (*Ficus microcarpa* Microcapa, *Delonix regia* Regia), Grass	2 side rows, Percentage of the ground covered by vegetation = {20%; 50%; 70%}	WS, AT
Gebert et al. (2019)	Melbourne, Australia	Cfb	N-S	Full	-	0.25 – 0.55	Trees (*Olea europaea*, *Eucalyptus olivacea*oltvacea)	2 side rows; Leaf Area Index = {1.13, 2.36}	AT, RH, VPD, LF, RAD, Gs, θv
Coutts et al. (2016)	Melbourne, Australia	Cfb	E-W	Full	-	0.27, 0.32, 0.76	Trees (*Platanus*, *Ulmus*)	2 side rows, Percentage of the ground covered by vegetation = {31%, 12%, 45%}	WS, AT, RH, RAD, UTCI
Gillner et al. (2015)	Dresden, Germany	Dfb	-	Full	-	-	Trees (*Aesculus* × *carnea*, *Corylus corluna*, *Ginkgo biloba*, *Liriodendron tulipifera*, *Tilia cordata*, *Ulmus x hollandica*) Trees (Aca, Cco, Gbi, Ltu, Tco, Uho)	Leaf Area Density = [0.90; 2.56]	AT, ST, RH, Gs, Emax
Andreou (2014)	Island of Tinos, Greece	Csa	Many	Full	-	Many	Trees	Height of Trees / Height of Building = [0.3; 1.0]	WS, AT, ST, RAD
Vailshery et al. (2013)	Bangalore, India	Cwa, Cfa	Many	Full	-	Many	-	Canopy cover = [30%;90%]-	AT, RH, ST
Djedjig et al. (2013)	La Rochelle, France	Cfb	N-S	Reduced	1/8	1.1	Green roofs and walls (sedum, mint, thyme…)	-	AT, RH, RAD, ST, HF
Correa et al. (2012)	Mendoza, Argentina	BWk	W-E	Full	-	0.16 – 0.31	Trees (*Platanus acerifolia*, *Morus alba*, *Fraxinus excelsior*)	2 side rows	WS, AT, RH, ST, RAD
Park et al. (2012)	Saitama, Japan	Cfa	-	Reduced	1/6	0.8	Trees	2 sides rows and 1 central row	WS, AT, GT
Ouldboukhitine et al. (2011)	La Rochelle, France	Cfb	N-S	Reduced	1/8	1.1	Green roofs (Tundra, Pampa)	-	AT, RH, LT, RAD
Shashua-Bar and Hoffman (2003)	Tel-Aviv, Israel	Csa	N-S, E-W	Full	-	0.3	Trees (*Ficus*)	2 sides rows, Percentage of the ground covered by vegetation = {63%; 74%}	WS, AT, LT, RAD

Table 2: Some studies carried out on vegetated canyon streets in outdoor environment. The scale of the street in a reduced environment is determined in relation to a reference height of 10 m. Variable names are AT: Air Temperature, Emax: Maximum evapotranspiration, Gs: Stomatal conductance, HF: Heat Flux, LHF: Latent Heat Flux, LT: Leaf Temperature, RAD: Radiation, RH: Relative Humidity, SHF: Sensible Heat Flux, ST: Surface Temperature, UTCI: Universal Thermal Climate Index, WS: Wind Speed. Climate characteristics refer to the Köppen-Geiger classification**:** BWk: Semi-arid climate, BWh: Arid climate, Cfa: Humid subtropical climates, Cfb: Oceanic climate, Csa: Mediterranean hot summer climates, Cwa: Dry-winter humid, subtropical climate, Dfa: Hot summer continental climates, Dfb: Warm summer continental or hemiboreal climates**.**

2 Materials and methods

2.1 Experimental site

For the purpose of the study, a canyon street was built at Institut Agro in Angers (47°28'N, 0°33'E), in north-western France. Angers has a temperate oceanic climate, considered as Cfb according to the Köppen-Geiger classification. The experimental installation consists of a 1/5 scale canyon street (Figure 1). The street is oriented north-south and prevailing winds are mainly from west, meaning that they blow perpendicular to the street. The street has nominal dimensions of 16 m long and 2 m wide. The two buildings which border it are 2 m high and 2 m wide. It can therefore be described as a "regular Canyon" since its aspect ratio (ratio of the height of the buildings to the width of the street) is 1. The floor on the ground of the canyon street consists, from top to bottom, of a 0.04 m thick layer of asphalt, a 0.25 m thick layer of gravel and a layer of brown soil beyond 0.25 m in depth. The walls are made of 0.1 m thick concrete and are insulated with 0.12 m thick expanded polystyrene and covered with white paint on the street-side. The roofs and external walls of the buildings were built with wooden frames and covered with steel pans to ensure rain proofness of the buildings.

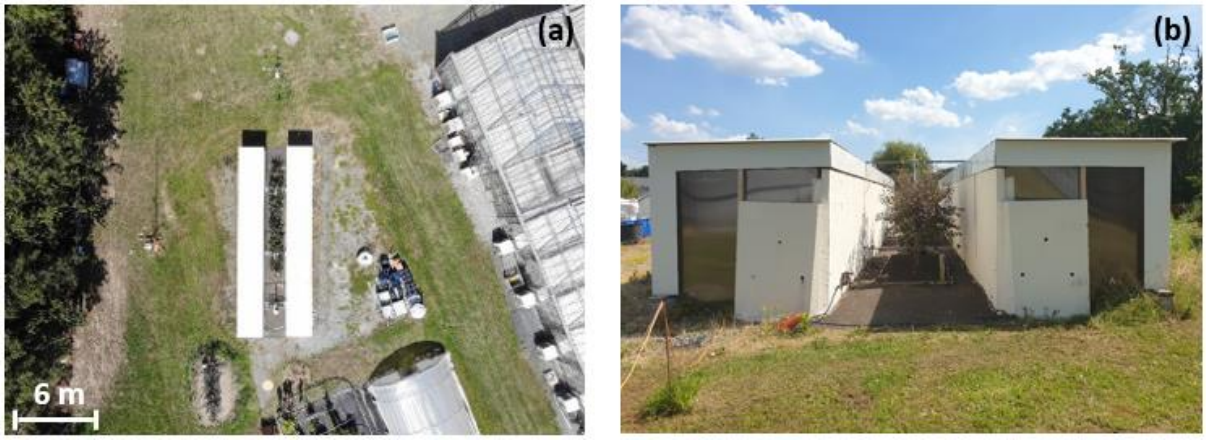

Figure 1 : Canyon street at 1/5 scale built at Institut Agro, in Angers (France). (a): top view, (b): front view Photo credit: INRAE, OPAALE research unit.

The street is divided into three modalities organized from north to south: a treed modality at the northern side of the street, a treed modality in the middle of the street and a treeless modality at the southern side of the street (see Figure 2). The existence of two vegetated modalities will enable us, in a future experiment, to grow the trees located in the middle of the street in condition of water restriction, in order to study the impact of the soil water availability on the climatic services provided by trees. However, in the present study, trees of both modalities were grown identically, in well-watered conditions. For this reason, in the present study only the Northern modality will be exploited for the vegetated condition and compared with the Southern non-vegetated modality. Each vegetated modality counts five trees, and all measurements were taken at the level of the three central trees, to avoid border effect.

The plant species used is the ornamental apple tree *Malus coccinella*® *'*Courtarou*'*. The studied trees are issued from cuttings, grown in a nursery (Briant Jeunes Plants) for 1 year. At the time of the experiment, the trees were 3-years old. They had been transferred one year earlier in the street in 80 L containers. The containers were filled with a layer of 0.25 m of topsoil/compost mixture in a 60/40 % volume ratio, followed at the bottom with a 0.1 m thick mixture of topsoil-compost/stone in a 65/35 % volume ratio. A layer of concrete with a slight slope was installed at the bottom of the containers to facilitate drainage. The total effective volume of the topsoil-compost mixture was finally 44.5 L. In cities, the trees are planted in pits with a volume of 10 m^3 (10,000 L), with 65 % of topsoil-compost mixture in volume ratio (the remaining 35 % corresponding to stones). This yields an effective volume of topsoil-compost of 6.5 m^3 at full-scale. Applying a geometrical reduction factor of $(1/5)^3$ gives an effective volume at

reduced-scale of 52 L. We can therefore see that the effective volume in our containers (44.5 L) is consistent with the value used in real cities. As for the choice of the 60/40 % proportions of the mixture of topsoil-compost, it is based on the common practices of green space planners (Bacholle et al., 2006). From a more scientific point of view, this ratio provides guarantees of the sustainable agronomic quality of urban soils supporting plantation trees. We have worked for several years on the effect of different doses of compost on soil structural properties (Cannavo et al., 2018, 2014; Vidal-Beaudet et al., 2012) showing that a proportion of 40 % compost by volume was the best compromise between the agronomic quality of the soil and tree growth.

2.2 Instrumentation

A scheme of the experimental facility with its equipment is shown in Figure 2. The experimental measurement campaign took place from June 8 to September 18, 2020. Sensors were installed inside the street in both vegetated and non-vegetated modalities and outside the street to measure a set of climatic variables: air temperature (in °C), relative air humidity (in %), wall temperatures (in °C), heat flux through walls (in W m^{-2}) and radiation (in W m^{-2}). Measurements of the climatic variables were also carried out outside the street using two meteorological masts. A 10 m high mast, located approximately 8 m west from the western building of the street, was equipped with sonic wind sensors at 2 m, 5 m, and 10 m from the ground to measure incident wind conditions on the street (recall that prevailing winds are coming from the west). A 2 m high mast, located approximately 6.5 m north from the northern end of the street, was used to measure temperature, humidity (at 0.4 m, 1.5 m, and 2 m from the ground) and radiation (at 2.1 m from the ground) conditions outside the street. The position of this Northern mast was chosen so that it benefits from the same incident insolation as the street. A Météo-France weather station is located about 400 m from the canyon street site. The trends of the data provided by this station and those of the data recorded next to the canyon street on the northern mast have been compared and show good consistency.

To quantify the impact of trees on the radiation budget of the street, 4-component net radiometer sensors were installed above each modality at 2.1 m from the ground. These radiation sensors provide access to the short and long wavelengths of ingoing and outgoing radiation. A net radiation sensor was also placed on the north mast at 2.1 m from the ground to measure the net radiation outside the street. Upward pointing pyranometers were placed in the center of the street, at 0.4 m from the ground, respectively in the non-vegetated modality and in the vegetated modality. These sensors measure the global radiation transmitted at 0.4 m and will allow to calculate, from the global radiation measured at 2.1 m, the rate of solar radiation intercepted by the buildings on the street on the one side, and by the walls and trees on the other side. Fluxmeters were installed 1 m from the ground on the east and west walls in each of the vegetated and non-vegetated modalities to measure both conductive heat flux through the walls and wall temperatures.

To measure the air temperature and relative humidity, temperature, and humidity sensors (TRH) sensors were installed in the vegetated and non-vegetated modalities as shown in Figure 2. A preliminary field survey revealed that a vertical gradient of air temperature and relative humidity develops, while gradients on the horizontal transverse axes only exist near the ground. For these reasons, the TRH sensors were placed on a vertical axis at 0.4 m, 1 m, 1.5 m, and 2 m from the ground. We also plan to evaluate thermal comfort at human being's height which, on the scale of the canyon street, corresponds to a height of 0.4 m. To do this, three TRH sensors were installed on the horizontal axis at 0.4 m from the ground respectively at 0.15 m from the west wall, in the middle of the street and at 0.15 m from the east wall. The air temperature and relative humidity data provided by the TRH sensors made it possible to calculate the absolute humidity.

To evaluate the heat stress felt outside the street and inside the street in both the vegetated and non-vegetated modalities, the UTCI (Bröde et al., 2012) comfort index was retained because compared to

other thermal comfort indices, it has the particularity of taking account of all climatic variables, to make use of an advanced human physiological model (Fiala, 2010), and to be valid for a wide range of climatic conditions. A globe temperature sensor was therefore installed at 0.4 m from ground outside the street (near the north mast) and inside the street in the non-vegetated and vegetated modalities. Together with the air temperature, humidity and wind speed respectively measured at the same height, the globe temperature will make it possible to evaluate the human comfort indices at 0.4 m, corresponding to a height of 2 m at full-scale, which is relevant for the evaluation of the thermal comfort.

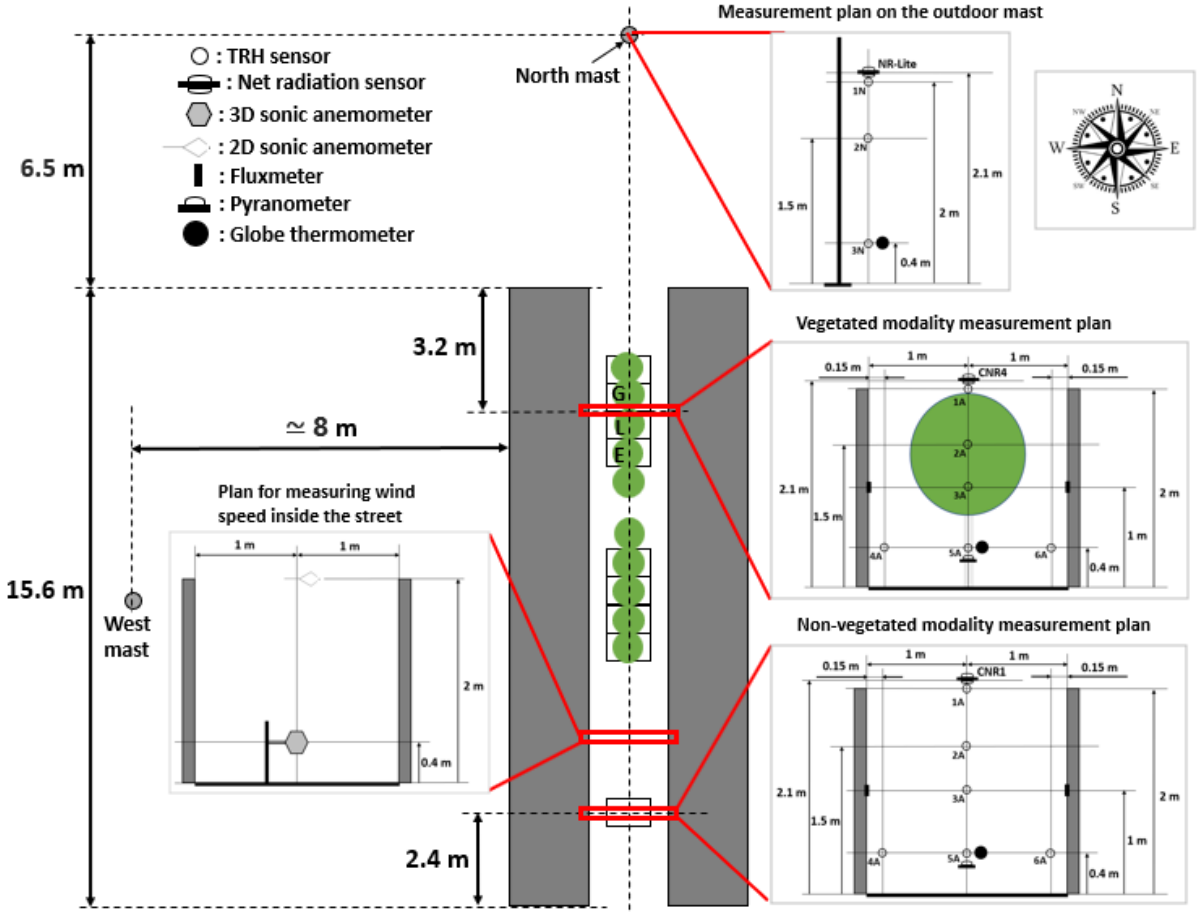

Figure 2 : Sketch of the street with the different modalities, the different measurement plans, the location of the different sensors and the outside masts. The positions of the trees are shown by green discs. Only tree marked G, L et E are investigated.

Each container was covered with an appropriate lid to prevent any water input from a rain event, and irrigation was ensured by sets of 4 drippers of 1 L per hour installed in each container. This arrangement makes it possible to control the water intake of the trees, which could be adjusted depending on the weather demand and on the tree development. In order to be able to carry out the water balance and monitor the soil water status, soil moisture sensors and tensiometers were installed in the three central containers of each modality to measure the soil volumetric water content and the soil water potential respectively. The location of those sensors is shown in Figure 3. Water potential measurements were performed at two depths (0.15 m and 0.3 m) and on both sides of the trees, to correctly evaluate water availability in the container. Water volumetric content was assessed at mid-depth (at 0.22 m) using capacitive ECH2O sensors located in the North and South of the containers. The sensors were calibrated in the lab using the same soil mixture as in the container. The data from the soil sensors were analyzed and confirmed that all the trees were well-watered during all the measurement campaign: indeed, soil water potential was often close to field capacity (-330 hPa), and always stayed above -800 hPa, ensuring

well-watered conditions. Moreover, a daily observation of drainage confirmed that irrigation was abundant enough to ensure trees were well-watered. The characteristics of the sensors we used are provided in Table 3.

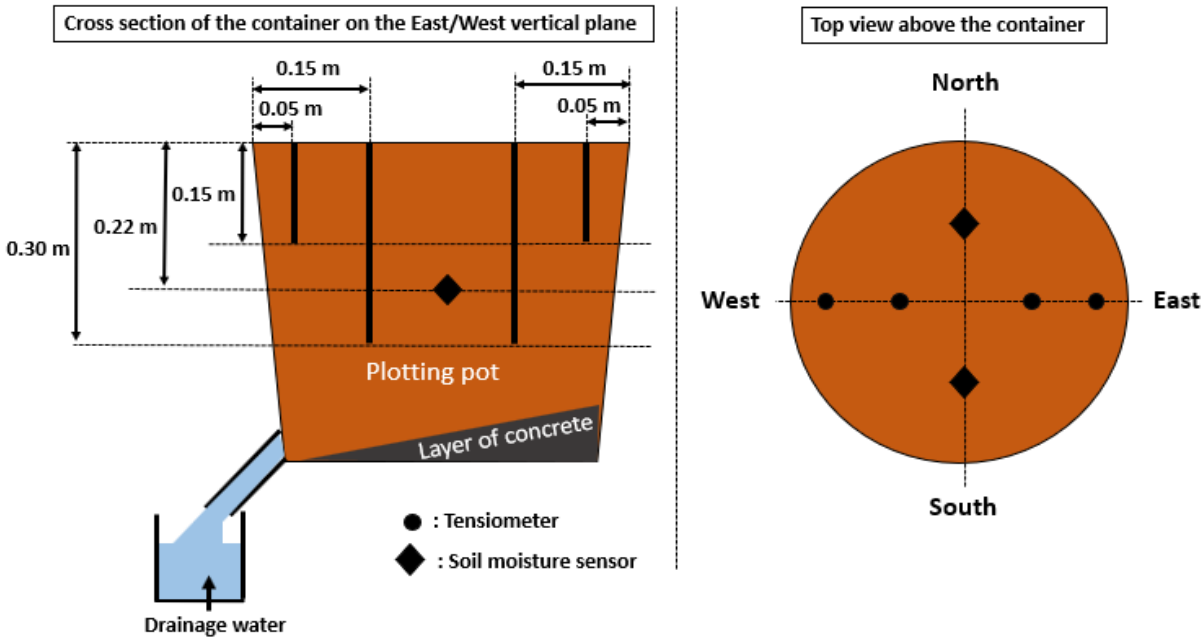

Figure 3 : Location of soil sensors in the three central containers of the vegetated modality.

Measured variable	Sensor type	Measurement range	Accuracy	Reference, manufacturer
Wind speed & wind direction (street: z = 0.4 m)	3D sonic anemometer	0 to 30 m s^{-1} 0-359°	0.08 m s^{-1} ±0.7° à 1 m s^{-1}	CSAT3, Campbell Scientific Ltd
Wind speed & wind direction (west mast, z = 10 m)	2D sonic anemometer	0 to 60 m s^{-1} 0-359°	± 2% à 12 m s^{-1} +/- 3° à 12 m s^{-1}	Wind Sonic, Gill instrument
Wind speed & wind direction (west mast: z = 2 m and z = 5 m; street: z = 2 m)	2D sonic anemometer	0.25 to 40 m s^{-}	± 0.13 m s^{-1} ± 1.5°	CV7, LCJ
Solar and long wavelength radiation	Net radiometer		10 %	CNR1, CNR4, and NR-Lite, Kipp & Zonen,
Surface temperature	Flat platinum probe	-	0.1 °C	PT100, TC ONLINE
Surface temperature	Fluxmeter	-30 to 70 °C	n.c.	Captec
Heat flux	Fluxmeter	Up to 150 kW	+/- 3 %	Captec
Air temperature (vegetated modality)	Platinum probe	-40 to 60 °C	±-0.2 °C	Pt1000 HMP110, Vaisala
Relative humidity (vegetated modality)	Capacitive probe	0 to 100 %	±1.5 % for HR ≤ 90 % ±2.5 % for HR > 90 %	Pt1000 HMP110, Vaisala
Air temperature (non-vegetated modality)	Platinum probe	-70 to 180 °C	±0.2 °C	Pt100 HMP337, Vaisala
Relative humidity (non-vegetated modality)	capacitive	0 to 100 %	± (1.0 + 0.008 x indicated value) % HR	Vaisala HMP337
Volumetric Water content	capacitive	0 to 100 %	±0.03 m^3 m^{-3}	ECH20 EC-5, Decagon

Table 3: Characteristics of the sensors used for experiments.

2.3 Methods

A description of the criteria and the method that were retained to choose the days for which collected data were analyzed is provided here. The way tree transpiration and street energy balance were operated are also described here. These preliminary calculations will then be used for data analysis.

2.3.1 Choice of investigated sunny and cloudy days

To choose these days, we first determined the relative sunshine on all days of the measurement campaign by calculating the ratio between the daily integral of the global radiation reaching the top of canyon street site, $R_{top-street}$ and the daily integral of solar radiation above the atmosphere, $R_{top-atm}$:

$$ratio = \frac{R_{top-street}}{R_{top-atm}} \qquad (1)$$

The daily integral of global radiation reaching the top of the canyon street is measured using the 4 components net radiometer located at 2.1 m from the ground of the street. The daily integral of solar radiation above the atmosphere, $R_{top-atm}, is$ given by:

$$R_{top-atm} = \frac{24 \times 60}{\pi} G_{sc} d_r [\omega_s \, sin(\varphi) \, sin(\delta) + cos(\varphi) \, sin(\delta) \, sin(\omega_s)] \qquad (2)$$

$R_{top-atm}$ is expressed in MJ m^{-2} day^{-1}. G_{sc} = *0.0820* MJ m^{-2} $minute^{-1}$ is the solar constant. φ is the latitude of the position in radian d_r, δ and ω_s are respectively the inverse of the relative (no unit) Earth-Sun distance, the solar declination in radian and the sunset angle in radian. These variables are respectively determined by:

$$d_r = 1 + 0.033 \, cos\left(\frac{2\pi}{365} J\right) \qquad (3)$$

$$\delta = 0.409 \, sin\left(\frac{2\pi}{365} J - 1.39\right) \qquad (4)$$

$$\omega_s = arccos[-tan(\varphi) \, tan(\delta)] \qquad (5)$$

J is the number of the day in the year (*J = 1* for January 1st and *J = 365* or *J = 366* for December 31st). The latitude φ of the city of Angers is 47.47°N or 0.828 radian.

Based on the analysis of the measured global radiation during several days of the experiment, it was established that days with a sunshine ratio above 0.65 were sunny days, and that days with a sunshine ratio below 0.45 were cloudy days.

2.3.2 Richardson number and flow convection regime

Regarding the stability and the wind convection regime, the relative importance of the inertial forces and buoyancy forces can be assessed using the Richardson number, which is given by the following formula:

$$Ri = -gH \frac{(T_w - T_0)}{T_0} \frac{1}{{U_0}^2} \qquad (6)$$

T_w and T_0 are the wall and free-stream temperature in K respectively, U_0 is the free stream velocity in m s^{-1}, g is the acceleration of the gravity in m s^{-2}, and H is the building height in m.

Here, T_w is the average of the 6 temperatures measured on the walls and on the ground in the vegetated modality and in the non-vegetated modality, T_0 is the air temperature measured at a height of 2 m on the north mast, U_0 is the wind speed measured on the outside mast at 10 m from the ground. When the Richardson number is close to zero, the flow conditions are neutral, and the flow regime is forced

convection. When the Richardson number is above zero, the flow is stable. When the Richardson number is negative, the flow conditions are unstable, with forced convection when -1 ≤ Ri ≤ 0, mixed convection when -10 ≤ Ri ≤ -1 and natural convection when Ri ≤ -10.

2.3.3 Tree transpiration calculation

Since tree transpiration is one of the means by which trees modify the microclimate, it was investigated in the present study. A water balance was done to estimate the tree transpiration (Figure 4). The water balance equation in volume of water per unit time is written as follows:

$$P + I - \Delta S - ETR - D \pm R = 0 \qquad (7)$$

P is the total rainfall, I is the irrigation applied to the soil, ΔS is the change in water stock in the soil, ETR is effective evapotranspiration, D is drainage and R is runoff. Here, the containers are protected from the rain, and moreover the days selected for analysis int the present study were not rainy, therefore the rainfall and runoff are zero and evaporation from the ground is negligible. Evapotranspiration is then equal to tree transpiration. Transpiration occurs during daytime, according to the climatic demand.

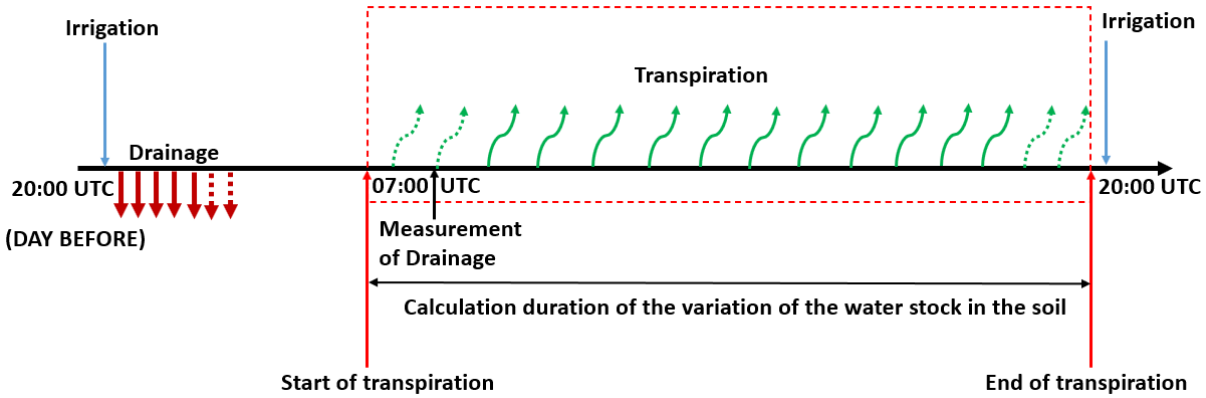

Figure 4 : Representation of the different stages of water inputs and outputs considered for the calculation of the water balance and transpiration amount.

The calculation period for tree transpiration was adjusted according to the sunlight duration and climatic demand of the day in order to match with the beginning and end of the transpiration period. Since irrigation occurs at 20:00 UTC, we can consider that drainage is finished before the sunrise and the start of the transpiration calculation. The water balance equation during the calculation period for transpiration then reduces to:

$$ETR = -\Delta S = -\Delta\theta \cdot V_{soil} \qquad (8)$$

$\Delta\theta$ is the change in volumetric water content computed using the two ECH2O sensors in each tree container, and V_{soil} is the volume of soil in each tree container. This time interval also presents the advantage of being free from possible uncertainties on irrigation or drainage measurement.

This real evapotranspiration, measured using the above-mentioned methodology, can be compared to a reference evapotranspiration ET_{ref}, which corresponds the evapotranspiration of a reference surface, defined as an extensive well-watered grass crop of 0.12 m height, with an albedo of 0.23, fully exposed to incident radiation. The reference evapotranspiration depends only on the climatic demand, and its expression is given by the so-called Penman-Monteith equation which results from the energy balance of the reference surface:

$$ET_{ref} = \frac{0.408\Delta\,(R_n - G) + \gamma\,\frac{900}{T+273}\,u_2\,(e_s - e_a)}{\Delta + \gamma(1 + 0.34\,u_2)} \qquad (9)$$

With ET_{ref}: the reference evapotranspiration in mm day^{-1}, Δ: slope of the water vapor saturation curve in kPa °C^{-1}, R_n: daily net radiation in MJ m^{-2} day^{-1}, G: conductive heat flux density in the ground in MJ m^{-2} day^{-1} usually considered as zero on a daily basis, γ: psychrometric constant in kPa °C^{-1}, T: mean daily air temperature in °C, u_2: mean daily wind velocity at 2 m from the ground in m s^{-1}, e_s: mean daily saturation pressure of water vapor in kPa, e_a: mean daily water vapor pressure in kPa.

A Meteo-France weather station provided daily values of ET_{ref}. Climatic variables measured on our meteorological masts also allow to compute a reference evapotranspiration for our experimental site.

The crop coefficient k_c of a given crop (other than grass) is given by the ratio of the ETR of that crop in well-watered conditions to ET_{ref}. The FAO-56 provides tabulated value of crop coefficients, for a wide range of agricultural crop, and at different growing stages. A common value if given for apple, cherry, and pear fruit trees. A mid-stage of growing season (which corresponds to the period of interest for this experiment), it reads: $k_{c0} = 0.90$. This value is valid for standard conditions of wind velocity and relative humidity over grass, namely u_2 = 2 m s^{-1} and RH_{min} = 45 %. Away from these conditions, the crop coefficient must be adjusted using the following formula:

$$k_{cb} = k_{cb0} + [0.04(u_2 - 2) - 0.004(RH_{min} - 45)]\left(\frac{h}{3}\right)^{0.3} \qquad (10)$$

Where k_{cb0}: crop coefficient under standard conditions, k_{cb}: crop coefficient under actual conditions, u_2: the mean value for daily wind speed at 2 m height over grass (m s^{-1}, for 1 m s$^{-1} \leq u_2 \leq$ 6 m s^{-1}), RH_{min}: the mean value for daily minimum relative humidity in (%) for 20 % $\leq RH_{min} \leq$ 80 %, h: the mean plant height in (m).

A different approach, the WUCOLS (Water Use Classifications of Landscape Species) approach, was proposed by the University of California Cooperative extension and the California department of water resources for estimating irrigation need of landscape planting (WUCOLS, 2000). Indeed, the FAO methodology is designed for food production, with the intention to maximize yield. In urban greening, the plant species may be different, and they are not grown with the same objective. In WUCOLS approach, the crop coefficient k_c is replaced by a landscape coefficient k_L, taking into account three factors through specific coefficients: the plant species coefficient (k_{plant}), the microclimate coefficient (k_{mc}), and the planting density coefficient ($k_{density}$). In well-watered conditions, we thus have:

$$ETR = k_L ET_{ref} \qquad (11)$$

$$k_L = k_{plant} k_{mc} k_{density} \qquad (12)$$

Different categories, each associated to a range of values, are proposed for each coefficient. Over 2700 landscape species are referenced, including crabapple tree, for which the plant factor is in the medium category, with an average value of 0.5.

2.3.4 Street energy balance

The energy balance was carried out over a 2.4 m long (corresponding to the sum of the width of the three pits containing the 3 central trees), 2 m wide (corresponding to the width of the street) and 2.1 m high (corresponding to the height of the net radiometer) volume inside the street deprived of trees (see Figure 5). The cumulated net radiation and conductive flux were calculated from the experimental values using the radiation and heat flux sensors installed in the non-vegetated modality. This energy balance may be written in the general form as:

$$R_n = G + H + L \qquad (13)$$

Where R_n is the net radiation, G the conductive flux density, H the sensible heat flux density and L the latent heat flux density (evapotranspiration). Since we perform the balance in the non-vegetated modality of the street, the latent term is therefore zero. The net radiation was computed using measurements from the net radiometer at z = H. The conductive heat flux density was computed as the sum of the conductive heat flux of the two walls and the ground. The sensible heat flux density can then be evaluated as the difference between the net radiation and the conductive heat flux. It must be stated that this estimation of the sensible heat flux as the residue of the energy balance is subject to caution as it can also be affected by uncertainties in the evaluation of the other terms.

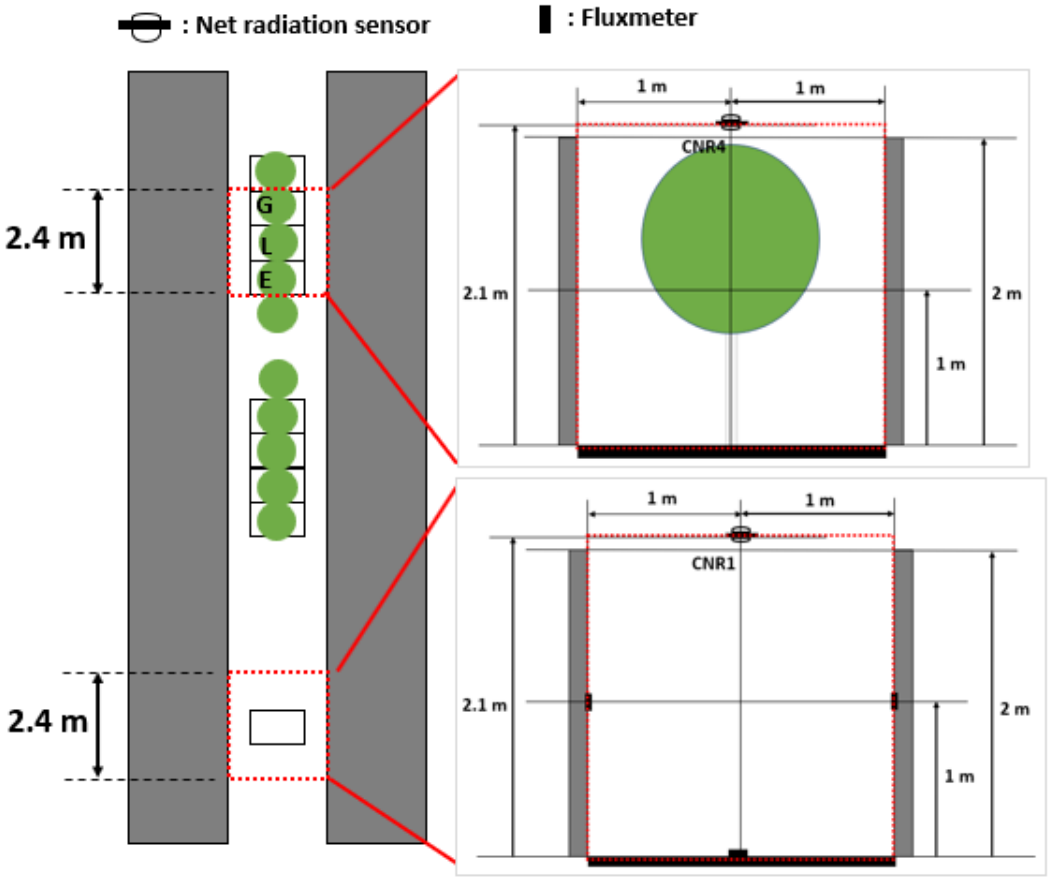

Figure 5 : Considered domains for the calculation of the energy balance in the non-vegetated modality and the transpiration of the 3 central trees in the vegetated modality.

3 Results

The results are analyzed according to two objectives:

- To study the impact of the canyon street on the microclimate by comparing the data acquired inside the street in the non-vegetated modality to those acquired outside the street using the north mast.
- To study the impact of trees on the microclimate inside the canyon street by comparing results acquired in the vegetated modality to those acquired in the non-vegetated modality of the canyon street.

3.1 Meteorological conditions during the selected days

For the purpose of the study, we will focus on two contrasting days in terms of solar radiation, but sufficiently close in time to have similar daylight duration and a stable leaf area for each tree. According

to the methodology described in section 2.3.1, July 25, 2020 presents a rather low value of this ratio (*ratio* = 0.243) and is therefore considered as a cloudy day. July 29, 2020 shows a relatively high ratio value (*ratio* = 0.655) and is therefore considered as a sunny day. July 29, 2020 was preceded by a very sunny day (*ratio* = 0.719), but July 25, 2020 was preceded by a moderately sunny day (*ratio* = 0.558). For the two studied days, the sunrise and sunset times were respectively 04:32 - 19:44 UTC for July 25, 2020 and 04:37 - 19:39 UTC for July 29, 2020.

The incident wind was analyzed using wind roses (not shown). For the two studied days, the direction of the incident winds was variable, but the wind speeds were very low on the experimental site (mostly lower than 2 m s^{-1} at 10 m from the ground). More specifically, the cloudy day direction (July 25, 2020) had clearly established southwesterly direction and a mean wind speed at 10 m of 1.3 m s^{-1}, and the sunny day (July 29, 2020) had a rotating northwesterly to northeasterly wind, with an average speed of 1.5 m s^{-1}. Regarding the flow convection regime, the daily evolution of the Richardson number, computed according to formula (6) in section 2.3.2. for the sunny day and for the cloudy day are shown in Figure 6. For the sunny day, we are in a mixed convection regime during the night (presence of thermal effects, negative values of Ri, down to -4) and in a forced convection regime during the day (close to thermal neutrality). On a cloudy day, we are almost always in forced convection and close to thermal neutrality.

Finally, the Penman Monteith reference evapotranspiration (ET_{ref}) (Allen et al., 1998) could also be calculated using the data from our meteorological mast (Eq. 9). It was 5.2 mm day^{-1} on July 29, 2020 and 1.7 mm day^{-1} on July 25, 2020.

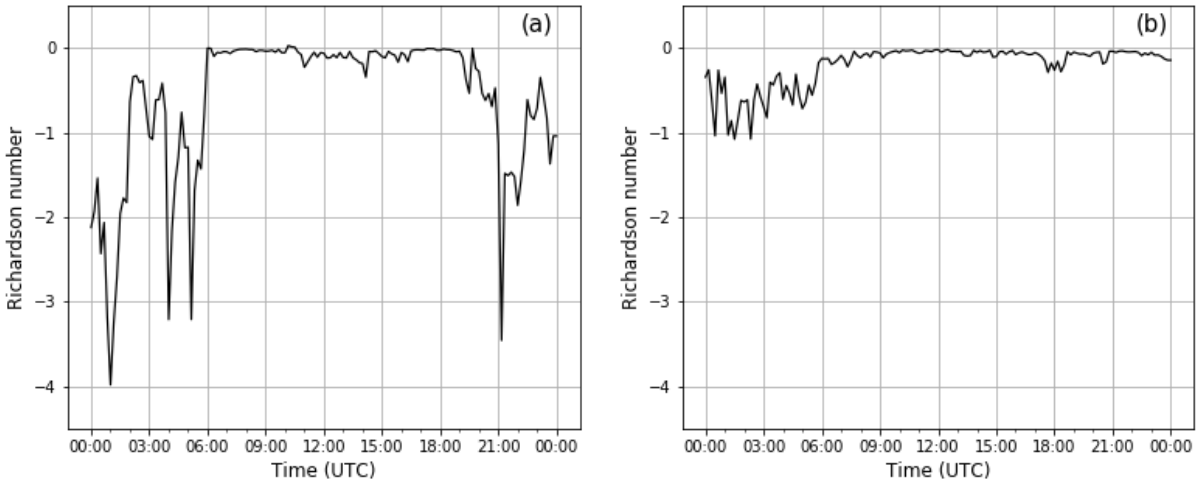

Figure 6 : Daily evolution of the Richardson number. (a): for the sunny day, (b): for the cloudy day.

3.2 Characteristics of the trees during the selected days

As far as the trees are concerned, the two selected days of investigation are sufficiently close in time to consider identical tree characteristics for the two days. The dimensions of the tree crowns were measured and the crown extended between 0.6 m and 1.7 m from the ground vertically, over 0.6 m on each side of the trunk laterally, and over 0.87 m longitudinally for each tree along the main axis of the street. This resulted in an average volume of 1.15 m^3 for each tree crown, and in a projected area of the tree crown of 1.04 m^2 per tree. The percentage of ground covered by vegetation, defined as the ratio of the projected area of the tree crowns by the total area of the street in the vegetated modality, is 60 %. One-sided leaf areas of the three trees in the center of the row in the vegetated modality were estimated on July 23, 2020 just before the studied days. The cumulated leaf surface area per tree was estimated using a leaf area allometric relationship and a coefficient of leaf surface area per unit length of branch (both

calibrated on our trees using reference leaves and reference branches), and then the measurement of all branches length for each tree. The total leaf areas values were 3.11; 2.53 and 2.14 m^2 for trees E, L and G, respectively, with an average value of 2.59 m^2 per tree (tree positions are shown in Figure 2 and Figure **5**). Compiled together with the crown dimensions, this yields an average Leaf Area Index (LAI) of 2.49 m^2 m^{-2} and an average Leaf Area Density (LAD) of 2.26 m^2 m^{-3}. The main parameters of interest are compiled in Table 4.

Projected area of crown (m^2)	Ground covered by vegetation (%)	LAI (m^2 m^{-2})	LAD (m^2 m^{-3})
1.04	60	2.49	2.26

Table 4: average characteristics of the street trees.

3.3 Radiation balance of the street

Quantifying the radiative phenomena that occur within the street is essential for the analysis of the urban over-heating and of the impact of trees on the microclimate. The daily evolutions of the different radiation components at 2.1 m high inside the canyon street in the vegetated and non-vegetated modalities are shown in Figure 7. The temporal dynamics of the different radiation components are similar in both modalities, both for the sunny and the cloudy day. Not surprisingly, the incident radiations (short and long wavelengths) are very similar.

On the sunny day, the "M" shape of the daily evolution of the reflected short wavelength radiation can be explained as follows:

- In the morning, the sun is in the East and the West wall mainly intercepts the solar radiation. The share of reflected short wavelength radiation is therefore important because of the rather high albedo of the white walls.
- Around midday, the sun is near the Zenith and it is the asphalt and the tree leaves (for the vegetated modality) that intercepts most of the incident solar radiation. As their albedo is lower than that of the white walls, the reflected short wavelength radiation is therefore less important. For the sunny day, the total albedos (ratio between reflected and incident short wavelength radiation for the street which combines reflection from the walls and depending on the modality from the ground and/or the trees) at 12:00 UTC in the non-vegetated and vegetated modality are 0.09 and 0.12 respectively. These quite low values can be explained by the fact that the sunny day at midday the reflected radiation comes mainly form the ground and/or the trees rather than from the white walls. These albedo values are consistent with the values between 0.1 and 0.12 for a sunny day found by Najjar et al. (2005) at the top of a canyon street in Strasbourg, with characteristics close to our experimental facility (aspect ratio of 0.9, north-east/south-west orientation, with very sparse vegetation) and also with the albedos of 0.12 without vegetation and between 0.11 and 0.12 with trees for a North-South oriented canyon modeled using TEB-Surfex in Redon (2017). In our study as well as in Redon (2017), the trees thus tend to increase the absorption of solar radiation in the canyon, thus slightly decreasing its albedo.
- In the afternoon, the sun is in the west direction and it is the east wall that is mainly exposed to the sun. The reflected short wavelength radiation increases due to the albedo of the wall.

For the cloudy day, the albedo values at 12:00 UTC are 0.19 and 0.18 in the non-vegetated and vegetated modality, respectively. These values are higher than during the sunny day because the radiation is more diffuse, and therefore a larger part is directed towards the white walls than during the sunny day.

On both the sunny and the cloudy days, the emitted long-wave radiation is larger than the incident long wave radiation, indicating that the street materials release their heat through long-wave radiation exchanges. Since the absorption of radiation is greater in the non-vegetated modality than in the vegetated modality, the emitted long wavelength radiation is greater in the non-vegetated modality

(37.88 MJ m^{-2} day^{-1} for the sunny day) than in the vegetated modality (36.56 MJ m^{-2} day^{-1}). This is also coherent with the surface temperatures that will be analyzed further. Finally, it can be seen for the sunny day that in the middle of the day (at 12:00 UTC), the net radiation in the vegetated modality is 49 W m^{-2} higher than the net radiation in the non-vegetated modality. At the same time, the net radiation measured outside of the street on the north mast is approximately 124 W m^{-2} higher than the net radiation in the non-vegetated modality (data not shown).

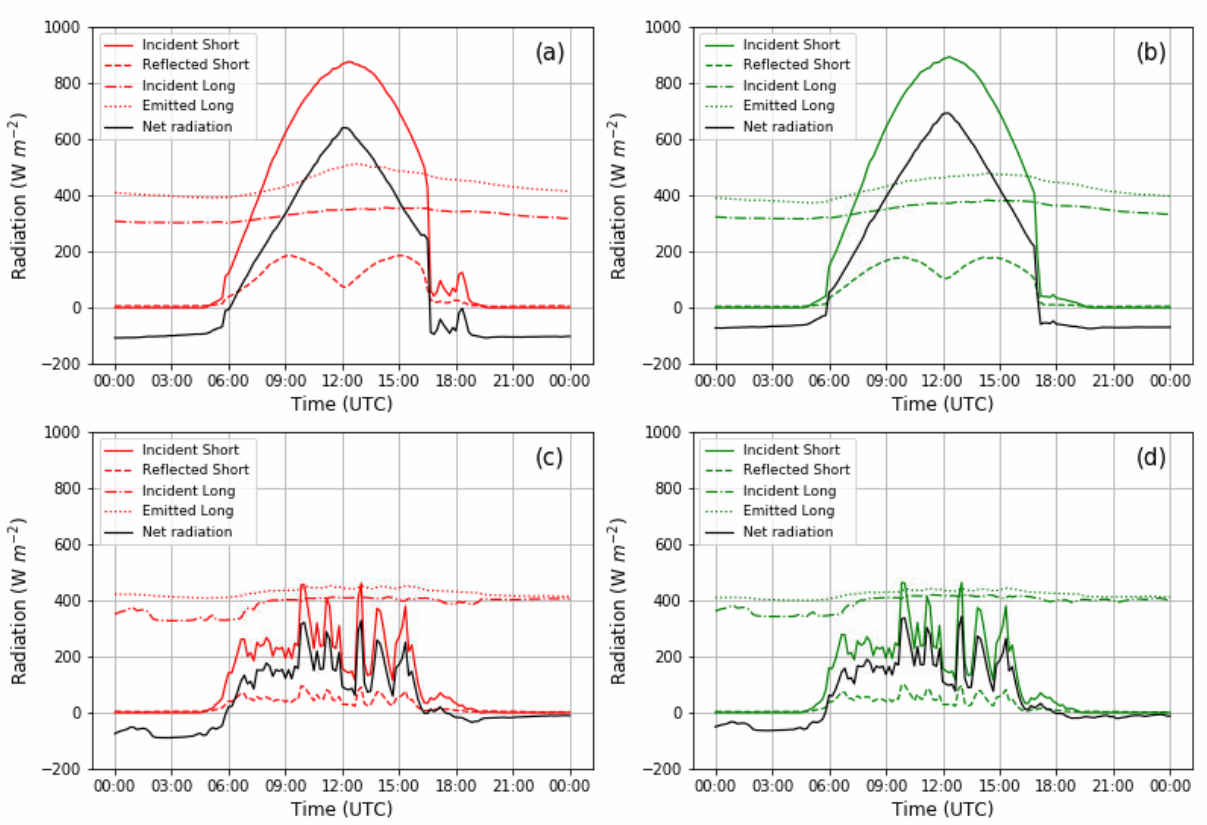

Figure 7 : Daily evolution of the different components of the radiation at 2.1 m height. (a): for the sunny day in the non-vegetated modality, (b): for the sunny day in the vegetated modality, (c): for the cloudy day in the non-vegetated modality, (d): for the cloudy day in the vegetated modality.

3.4 Interception of global incident radiation by the street and by the trees

The daily evolution of the incident global solar radiation inside the street (in the non-vegetated modality and in the vegetated modalities) at 2.1 m and 0.4 m from the ground is presented in Figure 8. Measurements of the overall incident solar radiation at 2.1 m confirm that the non-vegetated and vegetated modality of the street receive the same solar radiation. The measurement made at 0.4 m from the ground in the non-vegetated modality reflects the fact that the east and west walls of the street cause shading to the center of the street respectively during the morning (between 05:00 and 10:00 UTC) and during the afternoon (between 14:30 and 19:00 UTC). Andreou (2014) showed that north-south orientation provides indeed about 70 % of shading of the ground during summertime, for streets with an aspect ratio of 1. In the non-vegetated modality at 12:00 UTC, there is no more shading from the walls, and the global incident radiation measured at 0.4 m from the ground becomes slightly higher than the global incident radiation on the street (measured at 2.1 m from the ground), due to multiple reflections by the walls of the diffuse component of solar radiation (Kastendeuch et al., 2006). On a cloudy day, there is also an interception of the incident global radiation by the walls and trees, but this process is less pronounced than for the sunny day, mainly due to the diffuse character of the solar radiation.

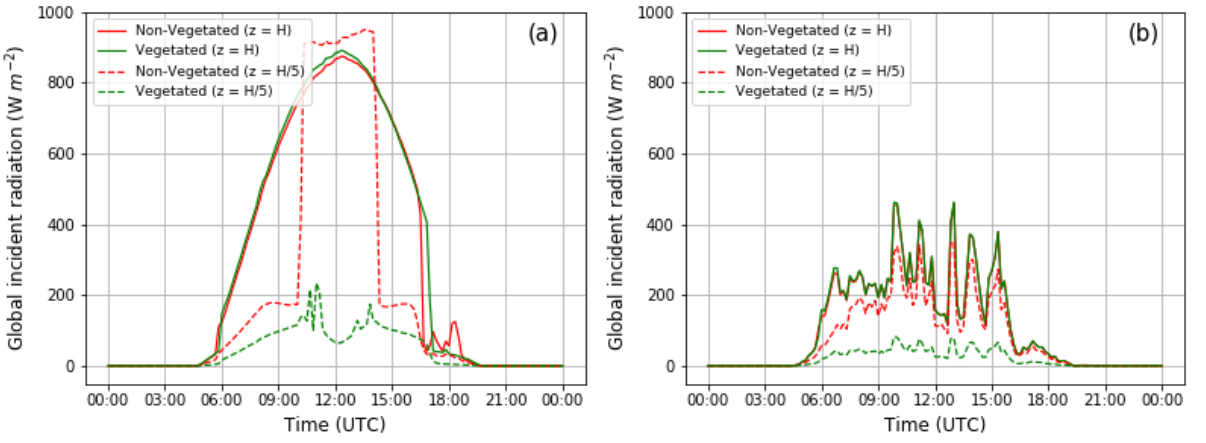

Figure 8 : Daily evolutions of global incident radiation in the non-vegetated and vegetated modalities of the street at z = H and z = H/5 (a): for the sunny day, (b): for the cloudy day.

The values of the one-day integrals of the incident global radiation at 2.1 m and 0.4 m respectively from the ground in the vegetated and non-vegetated street modalities are shown in Table 5. In the vegetated modality, the integral over the whole sunny day of the incident short wavelength radiation measured at 0.4 m from the ground (just below the trees) is 6.7 times lower than that measured at 2.1 m from the ground (just above the trees).

	At z = H (MJ m^{-2} day^{-1})	Non-vegetated modality at z = H/5 (MJ m^{-2} day^{-1})	Vegetated modality at z = H/5 (MJ m^{-2} day^{-1})	Difference at z = H/5 (MJ m^{-2} day^{-1})
Sunny day	25.27	17.09	3.75	13.34
Cloudy day	9.52	6.88	1.66	5.22

Table 5: Daily integral of incident global radiation at 2.1 m (z = H) and 0.4 m (z = H/5) from the ground in the vegetated and non-vegetated canyon street modalities for the sunny day and for the cloudy day.

For the sunny day, only 68 % of the energy arriving at the top of the street reaches the H/5 level in the non-vegetated modality, as a consequence of the shade provided by the walls, and only 15 % in the vegetated modality due to the combined interception of radiation by both walls and trees. 32 % of the energy arriving above the street is therefore intercepted by the walls (8.18 MJ m^{-2} day^{-1} of energy decrease) and 85 % of the incident energy is intercepted by the walls and trees. On a cloudy day, 28 % of the energy from the sun is intercepted by the walls but 83 % is intercepted by the walls and trees. Global incoming radiation at z = H is decreased at z = H/5, thanks to the tree shading, by 13.34 MJ m^{-2} day^{-1} on the sunny day, and by 5.22 MJ m^{-2} day^{-1} on the cloudy day. The parts of the incident energy intercepted by the trees for the sunny day and for the cloudy day is therefore 53 % and 55 %, respectively, meaning, from the energetic point of view, that the shading effect of the trees is therefore larger than that of the walls at H/5. These results also reveal very similar behaviors in terms of proportions of intercepted radiation by the trees both for the sunny and cloudy days.

3.5 Impact of the trees on wall fluxes and wall temperatures

The daily evolution of the heat fluxes on the east and west walls is presented in Figure 9. It can clearly be seen that the sun course has an impact on the heat fluxes. Trees reduced the heat flux on a sunny day by 99 W m^{-2} (maximum value) on the west wall and 76 W m^{-2} (maximum value) on the east wall.

Similar daily evolutions in wall temperatures are observed between the non-vegetated and vegetated modalities (Figure 10). For the sunny day, in the morning, the sun is in the east and therefore the west wall heats up rapidly to about 26.5 °C. The east wall temperature increases progressively during the

morning, and the reflection of incident solar radiation by the west wall probably contributes to this increase. In the afternoon, the sun is in the west and the temperature of the east wall, which is exposed to the sun, increases to about 34 °C. Thanks to the reflection of the radiation intercepted by the eastern wall, the western wall heats up again and its temperature reaches a second peak of about 27.5 °C.

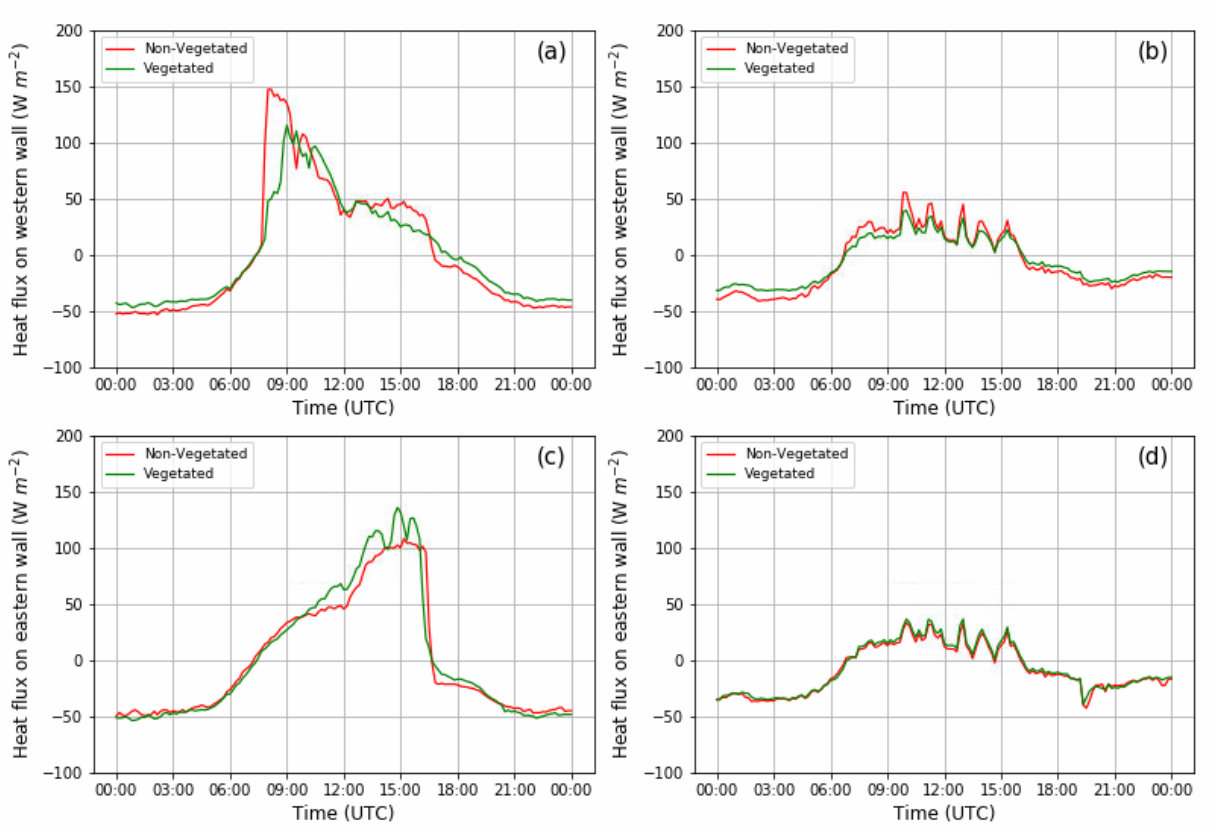

Figure 9 : Daily evolution of wall heat fluxes. (a): for the sunny day, western wall (b): for the cloudy day, western wall (c): for the sunny day, eastern wall (d): for the cloudy day, eastern wall.

As for the ground, it is observed that the more it faces the sun, the higher its temperature rises. The soil temperature in the non-vegetated modality rises up to 47 °C on the sunny day. These daily evolution of wall and ground temperature are very similar to that found by Najjar (2005). In their study, the ground temperature is the same (47 °C), while the wall temperatures are 2 °C higher for the eastern wall and 7 °C higher for the western wall. This difference on the walls may be due to the walls being less reflective in Najjar's street than in our experiment, and also to the street orientation which is 35° to the North in Najjar (2005). In contrast, the values of wall temperature obtained in Doya et al. (2012) in their North-South oriented canyon facility at the 1/8 scale in La Rochelle, France reach much higher values (60 °C for the eastern wall and 45 °C for the western wall), due to a dark paint on the wall with a very low albedo value (0.145). On a cloudy day, the temperatures of the east and west walls follow almost the same trend but are less impacted by the sun course, which is due, by the very low level of the direct component of the global radiation, as the sun radiation is mainly diffuse. We can finally notice that during the night, the ground cools down more during the sunny day (minimum of about 16 °C than during the cloudy day (minimum of about 19 °C). This is related to the fact that the sky is clearer on sunny days and that cooling by infrared radiation is more important. The effect of the interception of part of the incident global radiation by the trees is clearly visible on the wall temperatures. Indeed, Figure 10 shows that the trees contributed to maintain the east and west walls at temperatures lower by up to 7 °C and the ground at temperatures lower by up to 18 °C compared to the non-vegetated modality. These values correspond to differences at the time of temperature peaks. In their study, Gillner et al.

(2015) showed that, thanks to the shading effects, vegetation can reduce surface temperatures by 5.5 to 15.2 °C depending on the plant species used. The authors also showed that trees can reduce asphalt temperatures by up to 4.6 °C per unit of LAD (Leaf Area Density).

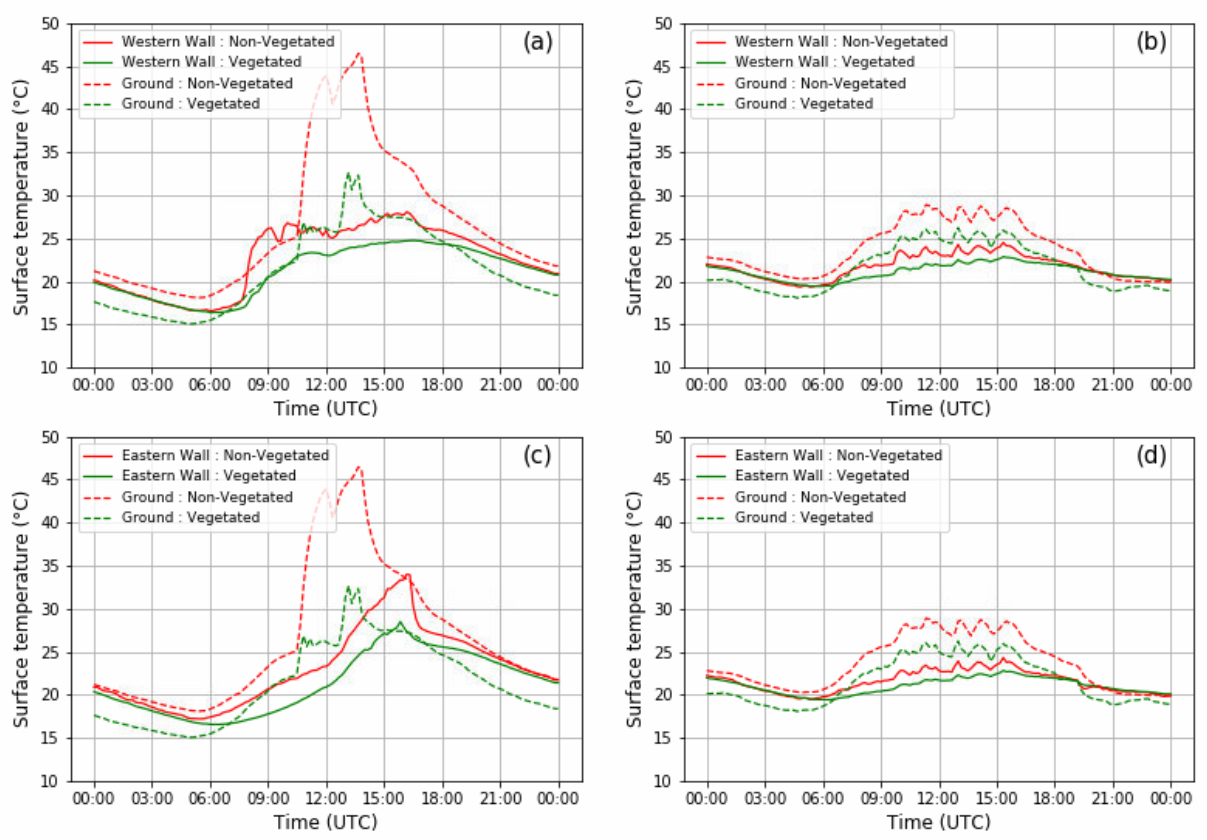

Figure 10 : Daily evolution of surface temperatures in the non-vegetated and vegetated modalities. (a): for the sunny day, west wall, and ground (b): for the cloudy day, west wall and ground (c): for the sunny day, east wall and ground (d): for the cloudy day, east wall and ground.

3.6 Tree transpiration

The daily evolution of the transpiration (Eq. 8) of the three central trees of the vegetated modality for the sunny day and for the cloudy day are respectively given in Figure 11 and Figure 12. The transpiration was calculated using the methodology described in section 2.3.3, with a transpiration period of 05:30-19:30 UTC for the sunny day and of 07:30-17:30 UTC for the cloudy day, because of the lower climatic demand in early morning and evening. For all trees, the daily evolution of evapotranspiration follows that of the incident global radiation, but with a certain delay for the sunny day, with a peak of transpiration at 14:00 UTC. This is probably due to the peak of air temperature occurring in the afternoon, and impacting the water vapor pressure deficit, which is another driver of transpiration. The daily cumulated transpiration of trees E, L and G is 2.4, 1.6 and 1.9 L day^{-1} respectively, for the sunny day (average value of 1.97 L day^{-1}) and 1.3, 0.6 and 1.2 L day^{-1}, respectively, for the cloudy day (average value of 1.03 L day^{-1}). Besides the indication already given in the Material and methods section on soil water potential during the whole experiment, the daily cumulated transpiration of the different trees also confirms that the irrigation of 4 L day^{-1} per tree for these two specific days was largely sufficient to maintain well-watered conditions for the two studied days. Using the projected area of the tree crown given in section 3.2, the tree transpiration can also be expressed in L m^{-2} day^{-1}, that is in mm day^{-1}: the average value is 1.9 mm day^{-1} for the sunny day and 0.99 mm day^{-1} for the cloudy day. Recall that reference evapotranspiration was 5.2 mm day^{-1} and 1.7 mm day^{-1}on the sunny and cloudy day,

respectively. The ratio of real to reference transpiration gives a crop coefficient of 0.37 (for the sunny day) and 0.58 (for the cloudy day) for our ornamental apple trees. The FAO-56 crop coefficient for the apple tree is 0.9 during mid-season under standard conditions. Adjusted for the weather conditions of the specific days investigated, it reads 0.93 for the sunny day and 0.83 for the cloudy day. It is of interest to note that the transpiration of our trees in urban condition is therefore lower than the theoretical one predicted by FAO. Two main reasons can be invoked: first of all, the FAO deals with agricultural crop, with the aim to maximize yields. Here, we are in a different perspective: our apple trees are young ornamental trees, the fruits are not edible, and for this reason the FAO crop coefficient may be overestimated here. Secondly, the growing conditions are not optimal in our street in terms of solar access of the trees. As reported in the literature (Andreou 2014), the north-south orientation in summer provides a lot of shade inside canyon streets; and the sun global radiation is the main driver for transpiration. This may also explain why the crop coefficient we obtain is higher for the cloudy than for the sunny day: being already in the shade from the cloud cover of the sky, the street does not bring additional shade to the street during the cloudy day. Therefore, the crop coefficient based on our transpiration measurements during the cloudy day is closer to that of FAO-56 than the one for the sunny day.

When applying the WUCOLS method proposed in WUCOLS (2000) (see section 2.3.3) for landscape planting, we consider an average planting density with a value $k_{density} = 1$. The crabapple tree has a lower plant coefficient ($k_{plant} = 0.5$) than that of orchard tree in FAO. For the cloudy day, considering that the shading effect of the walls is reduced, the microclimate falls into the higher end of the "low" category, with $k_{mc} = 0.9$. This gives for the cloudy day a landscape coefficient $k_L = 1 \times 0.5 \times 0.9 = 0.45$. This value is quite close to the one we obtain for cloudy day (0.58). During the sunny day, due to the shading from the walls, our street falls into the middle of the "low" category for the microclimate coefficient, with $k_{mc} = 0.7$. According to the WUCOLS approach, the landscape coefficient thus reads $k_L = 1 \times 0.5 \times 0.7 = 0.35$, which is close to our value for the sunny day (0.37). Therefore, the WUCOLS (2000) approach present a better match to our results than that of FAO approach, by taking into account the ornamental species investigated (crabapple tree), the landscape application, and the microclimate of the street.

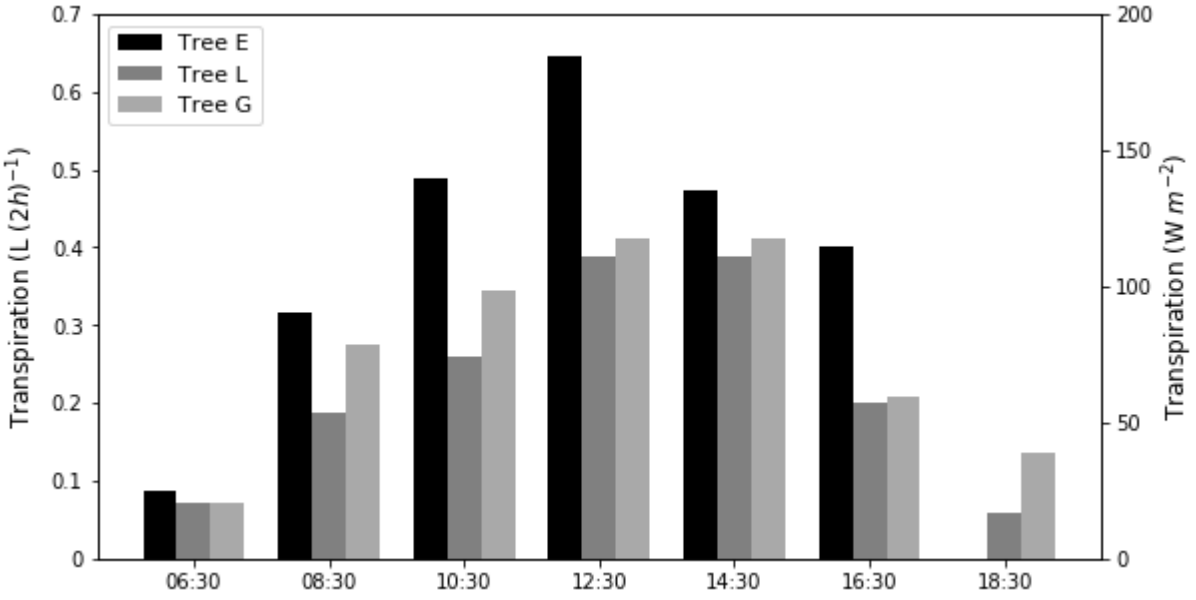

Figure 11 : Transpiration of the three central trees (E, L and G) of the vegetated modality for the sunny day.

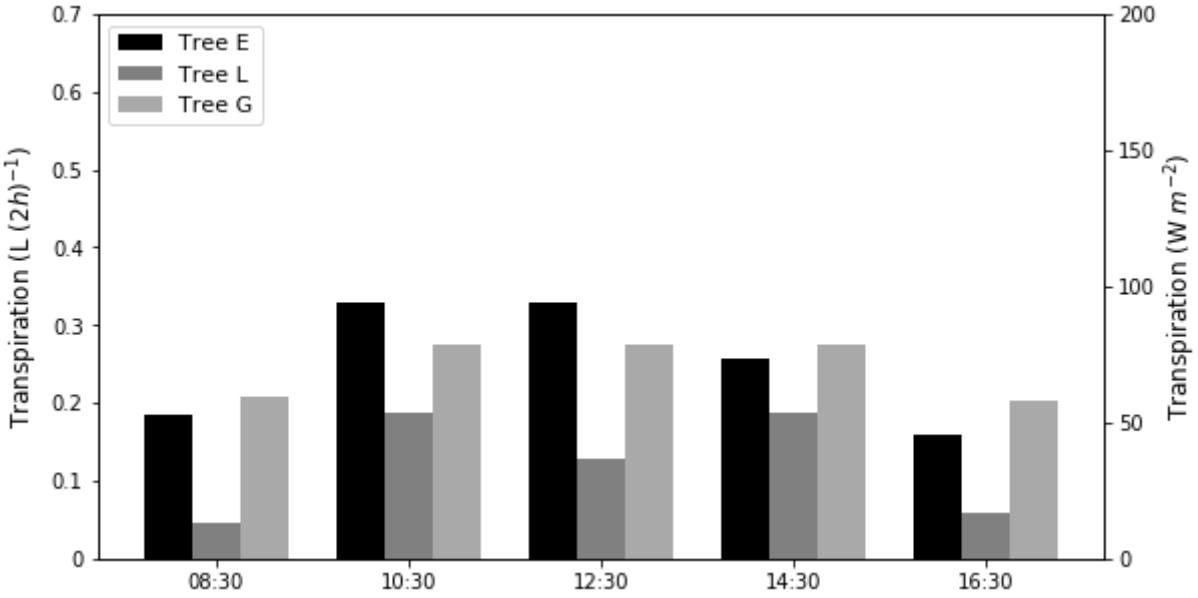

Figure 12 : Transpiration of the three central trees (E, L and G) of the vegetated modality for the cloudy day.

From the energetic point of view, multiplying by the latent heat of vaporization of water at 20 °C (L_v = 2.46 MJ kg^{-1}) yields a transpiration of 4.66 MJ m^{-2} day^{-1} and 2.44 MJ m^{-2} day^{-1} during the sunny and the cloudy day, respectively. These figures will be compared in the discussion section (section 4.) to the reduction of global radiation provided by the trees, in order to compare the relative impact of shading and transpiration in climatic benefits of the trees.

3.7 Impact of the street and trees on air temperature

The spatial distribution of air temperature along the central vertical axes of the non-vegetated and vegetated canyon street modalities is presented in Figure 13. It is generally observed that the distribution of the air temperature is almost uniform during the night (at 03:00 UTC) for both sunny day and cloudy day. On the central vertical axis, for both the sunny day and the cloudy day, it is observed that, for the sunny day, the air temperature measured under the canopy at z = 0.4 m during the day (12:00 UTC) is lower by 2.7 °C than that measured in the non-vegetated modality at the same height thanks to shading caused by the trees.

Since the impact of trees on air temperature appears to be greater under the canopy than at other locations inside the street on the sunny day, we now turn our attention to the spatial distribution of air temperature on the transverse horizontal axis located 0.4 m from the ground as shown in Figure 14. This height is also of interest for the evaluation of thermal comfort. Again, for the sunny day and for the cloudy day, we observe almost no difference between the two modalities of the street during the night (at 03:00 UTC). The spatial distribution of air temperature is almost uniform. At 12:00 UTC, we notice that it is cooler (by 2.7 °C) in the vegetated modality compared with the non-vegetated one in the sunny day, especially under the tree crown in the middle of the street (x = 1 m).

The daily evolution of air temperatures outside the street and inside the street at z = 0.4 m = H/5 from the ground (in vegetated and non-vegetated modalities) and at mid-distance from the walls, are presented in Figure 15. Globally, it can be noted that for both types of studied days, the air temperature at z = H/5 follows almost similar temporal evolutions. It increases from around 05:00, shortly after sunrise, reaches a maximum around 14:00 and decreases from 18:00 onwards because of reduced solar radiation. Under the effect of solar radiation, which heats up the walls and the air more during the day, and of a clearer sky at night, which allows a more important cooling by long wavelength exchange, the sunny day shows

a daily amplitude of the variation of the air temperature (approximately 18 °C over the day) much larger than for the cloudy day (approximately 8 °C over the day).

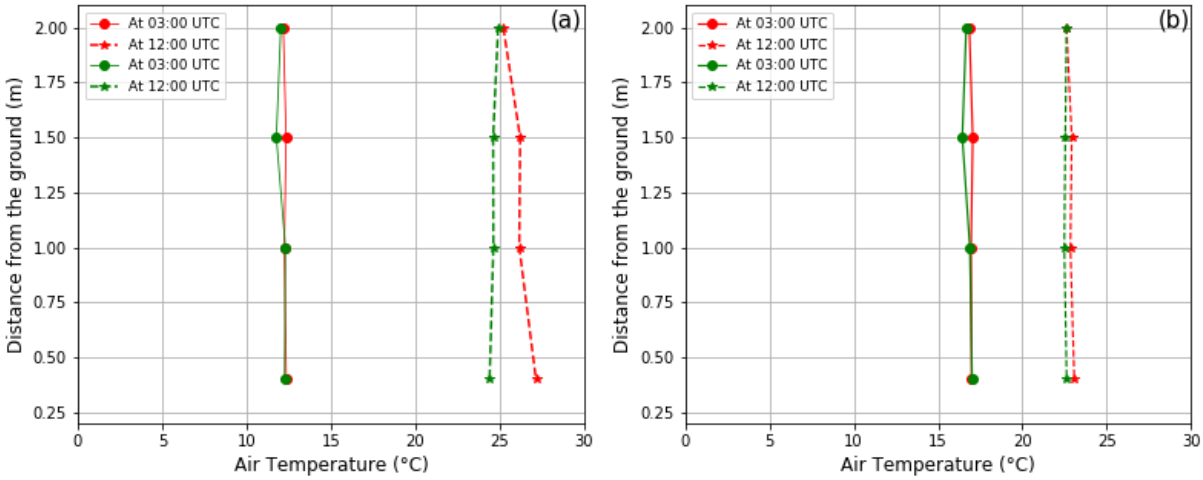

Figure 13 : Vertical distribution of air temperature on the central vertical axis. (a): for the sunny day, (b): for the cloudy day. The non-vegetated modality and vegetated modalities are represented in red and green color respectively.

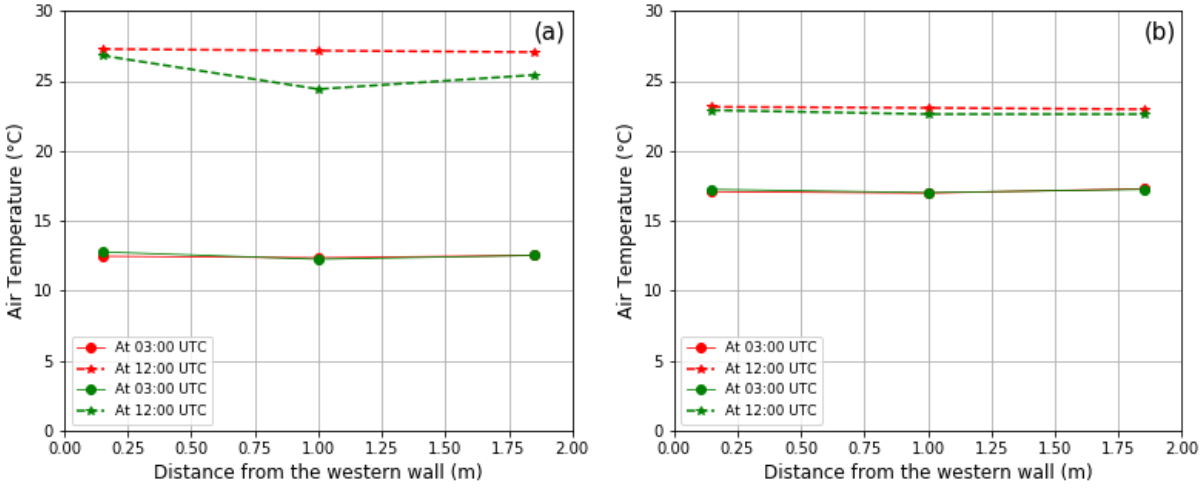

Figure 14 : Horizontal distribution of air temperature on the transverse horizontal axis at 0.4 m from the ground. (a): for the sunny day, (b): for the cloudy day. The non-vegetated modality and vegetated modalities are represented in red and green color respectively.

In order to better visualize the impact of the street on the microclimate on the one hand, and the impact of trees on the microclimate in the street on the other hand, the temperature differences between modalities are also presented in Figure 15. Concerning the sunny day, at 0.4 m from the ground, the air temperature in the street remained higher than outside the street by up to 2.1 °C (maximum value) during the night until 06:00 due to the release of the heat that had been stored by the street materials during the day, thus highlighting the phenomenon of urban overheating at night. In the early morning, from 06:00 to 10:00 UTC, the inertia of the materials in the street causes the air inside the street to heat up slower than the air outside the street, creating an island of coolness inside the street of 0.9 °C (maximum value). From 11:00, the phenomenon of urban overheating occurred again (with a maximum overheating of 2.4 °C). But the temperature of the outside air became slightly higher (by 0.5 °C) than that inside the street from 15:00 to 18:00 UTC, due to the shading produced by the west wall at 0.4 m (Table 5). We can see that the intensity of urban overheating gradually increases with the arrival of night before

reaching a level around 2 °C, very close to the value obtained the night before. We can also observe that the trees reduced the temperature inside the street and that this reduction is greater on a sunny day than on a cloudy day, thus highlighting the trees' ability to cool the air through the phenomenon of transpiration and shading. At 0.4 m above the ground level, trees reduced the air temperature inside the street by 2.7 °C (maximum value at 12:00 UTC) on a sunny day and by 1.2 °C (maximum value at 13:00 UTC) on a cloudy day.

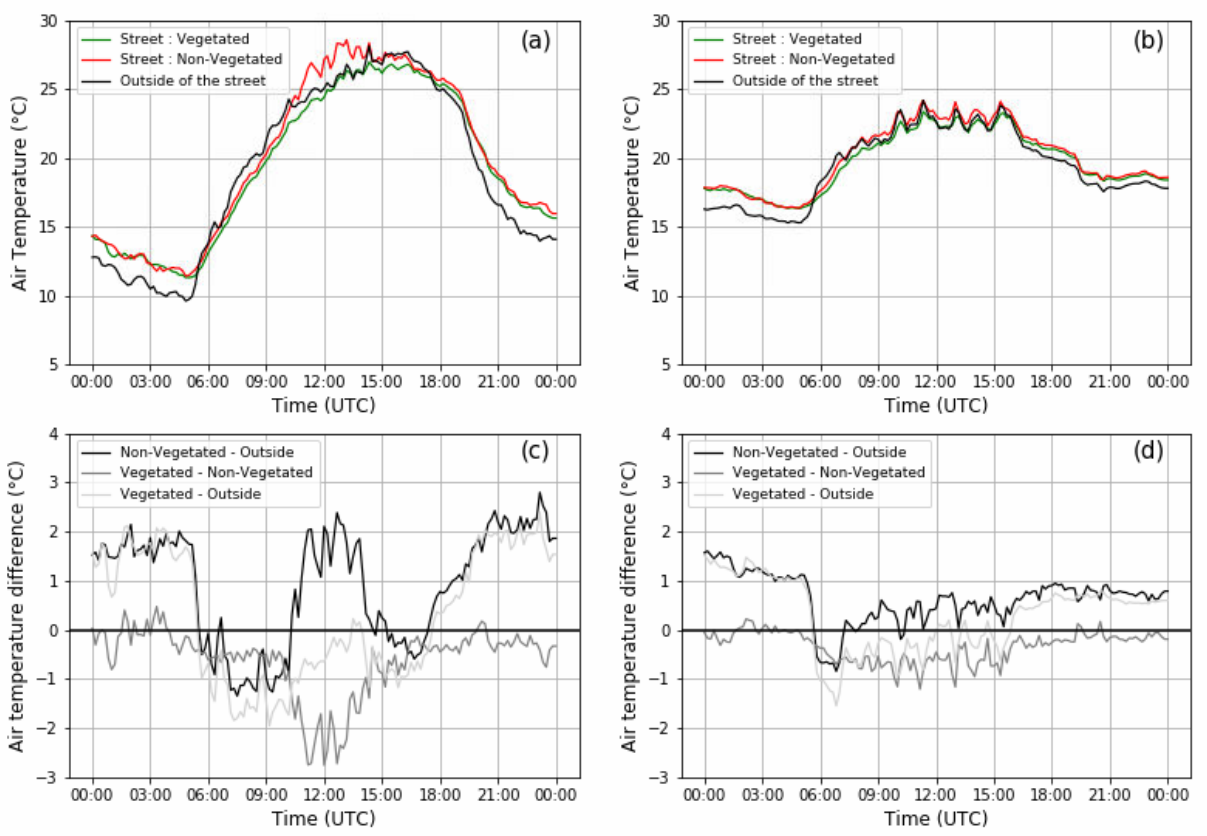

Figure 15 : Daily evolution of air temperatures outside and inside the street at 0.4 m from the ground and at mid-distance from the walls. (a) and (c): for the sunny day, (b) and (d): for the cloudy day.

The air temperatures presented in Figure 15 indicate that the street creates urban overheating. Experimental data also showed that the street is cooler in the morning. The morning coolness observed in the street on sunny days is a phenomenon that is not well known in the literature but has also been observed by Oke et al. (2017) and in the city of Lyon by Lauzet (2019). On the impact of the urban environment on the microclimate, we noted for the sunny day a maximum difference of 2.1 °C between the air temperature inside the non-vegetated street measured at 0.4 m from the ground (at z = H/5) and the air temperature outside the street measured at the same height. A difference of about 2.5 °C during daytime between the air temperature at the center (at z = H/2) of a canyon street (Scale = 1/8; Aspect Ratio = 1) and the air temperature above the street (at z = 2H) was measured by Wang et al. (2017), which is very close to our result (2.4 °C) for the sunny day. Surprisingly, Wang et al. (2017) do not measure any significant urban overheating at night. Doya et al. (2012) observed a maximum difference of about 5 °C during daytime and a difference of about 1.5 °C during nighttime between the air temperature in the street (which they called "Control Street") and the air temperature measured above a 16 m high building. Therefore, the urban overheating obtained by Doya et al. (2012) is much higher during the day, but slightly lower during the night. This difference in day-time overheating is linked to differences in the wall temperatures, which reach up much higher values in Doya et al. (2012) (60 °C)

due to a very low albedo value of the paint on the walls (0.145). Moreover, in Doya et al. (2012), the air temperature in the street is measured near a warm wall (at a height of H/2). Finally, regarding the strong decrease in urban over-heating observed in our street between 15:00 and 18:00 UTC that we explained with the shading provided by the east wall, we can question whether it would be as strong at full-scale in a real city. Indeed, our experimental facility consists in an isolated street oriented north-south, and shading from the building walls is reputed important for this orientation during summer time (Andreou, 2014). In a full city, the temperature inside a street is also influenced by the temperature in the surrounding streets, and the different street orientations can therefore in part compensate each other.

On the impact of trees on the air temperature inside the canyon street, the analysis of our experimental data clearly showed that trees help fight against overheating in the street, since they reduce the air temperature up to 2.7 °C (maximum value), thus allowing to do more than compensate for the overheating (whose maximum value was 2.1 °C during the night). The benefits of trees in terms of air temperature reduction that we observed are of the same order of magnitude as those reported in the literature. Indeed, a synthesis study carried out by Qiu et al. (2013) shows that vegetation can reduce the air temperature of the surrounding environment by 0.5 °C to 4 °C depending on the season, the vegetalization solution and the plant species. It has also been shown that, compared to a non-vegetated surrounding area, vegetation can reduce air temperature by 0.4 to 6 °C according to Coutts et al. (2016), up to 2.5 °C according to Bowler et al. (2010), by 0.7 to 2.2 °C according to Gillner et al. (2015), by 1.5 to 5.6 °C according to Jamei et al. (2016) and up to 1 °C according to Shashua-Bar and Hoffman (2003).

3.8 Impact of the street and trees on air relative and absolute humidity

The daily evolution of relative humidities outside the street and inside the street (in vegetated and non-vegetated modalities) are presented in Figure 16. Again, as for air temperatures, relative humidities show globally similar evolutions at 0.4 m from the ground for both sunny and cloudy days. They decrease from 06:00 UTC (just after sunrise), reach their minimum around 18:00 UTC and then increase again with the effect of sunset. This evolution is coherent with that of air temperature (see Figure 15), given the fact that the saturation pressure increases with air temperature. The range of relative humidity variations is from 30 to 95 % for the sunny day and from 60 to 95 % for the cloudy day. It can be observed that, overall, the canyon street decreases relative humidity compared to the outside air. As for trees, it can clearly be observed that they play a role in the increase of the relative air humidity in the canyon street, but only during daytime, which is the period when transpiration occurs.

The analysis that was done on the spatial distribution of relative humidity and absolute air humidity (data not shown) with that of air temperature led to the conclusion that spatial variations in relative air humidity are mostly due to variations in absolute humidities. Figure 17 shows that the daily evolutions of absolute humidity outside the street and inside the street (in vegetated and non-vegetated modalities) are also similar at 0.4 m from the ground. Absolute humidity changes along the day from 6 to 8.5 g of water per cubic meter of dry air on the sunny day and from 10 to 12.5 g of water per cubic meter of dry air on a cloudy day. For the sunny day, the absolute humidity increases in the morning to reach a maximum at 11:20 UTC, then decreases in the afternoon with a slight stall from around 14:20 UTC. This temporal evolution is consistent with the expected daily evolution of reference evapotranspiration (Allen et al., 1998), and the dynamics of the measured tree transpiration (cf Figure 11 and Figure 12 in section 3.6), which explains well this evolution for the outside the street and in the treed modality of the street. It can be noticed that the non-vegetated modality of the street follows the same overall evolution, but with milder gradients across the day. This can be explained by the mixing of ambient air between the different modalities of the street and the outside of the street, which bring some part of absolute humidity produced by transpiration into the non-vegetated modality.

During the sunny day, the absolute humidity is higher during the day by up to 0.5 g of water per cubic meter of dry air in the vegetated modality of the street and outside the street, compared to the non-

vegetated modality of the street, highlighting the effect of trees (inside the street) and grass (outside the street transpiration). In all three spaces, the absolute air humidity in the vegetated modality remains almost stable during the night, but it is noticeably higher (by up to 0.3 g of water per cubic meter of dry air) inside the street than outside the street. This trend towards an urban excess of humidity at night can be surprising, but it has been in fact consistently reported by several authors (Holmer and Eliasson, 1999; Tapper, 1990) as analyzed by Pigeon (2007), and could be attributed to a lower condensation at night in cities. Overall, the differences observed between the different modalities and time of the day remain small.

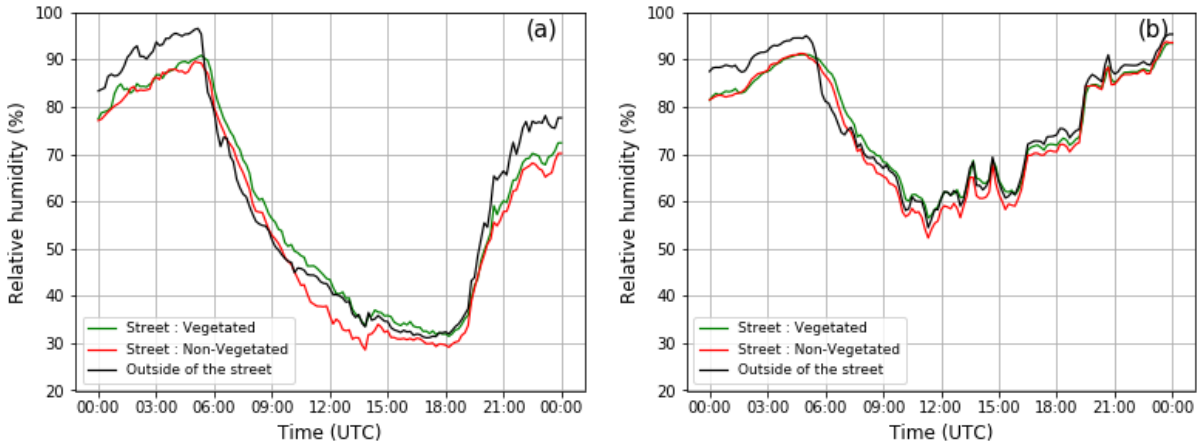

Figure 16 : Daily evolution of air relative humidities outside and inside of the street at 0.4 m from the ground. (a): for the sunny day, (b): for the cloudy day.

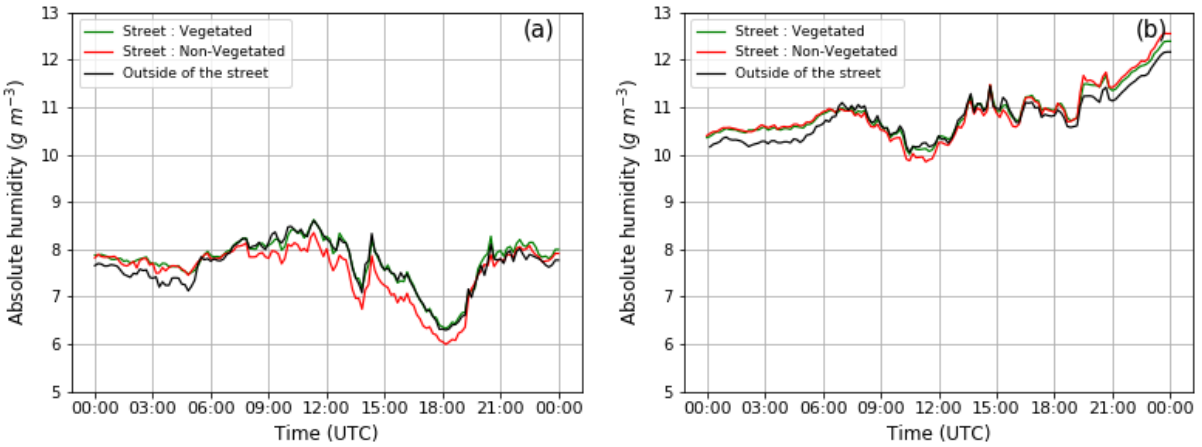

Figure 17 : Daily evolution of air absolute humidity outside and inside the street in the non-vegetated and vegetated modalities at 0.4 m from the ground. (a): for the sunny day, (b): for the cloudy day.

3.9 Impact of the street and the trees on Universal Thermal Climate Index (UTCI)

We used the Universal Thermal Climate Index to calculate the heat stress felt outside as well as inside the street in the vegetated and non-vegetated modalities. The different heat stress categories based on the UTCI may be found in Bröde et al. (2012). The daily changes in UTCI outside and inside the street calculated at z = 0.4 m (corresponding to human height at full-scale i.e. ~ 2 m) are given in Figure 18. During the night, the UTCI is 2.5 °C higher in the street than outside the street for the sunny day, and about 1.5 °C higher during the cloudy day. At this period of the day, there is very little difference between the vegetated and non-vegetated modality. Indeed, at night, the trees do not provide cooling through shading and transpiration. However, trees are sometimes reported to prevent longwave radiation

cooling at night due to a reduced sky-view-factor. In our results, the UTCI value of the vegetated modality at night is slightly higher than in the non-vegetated modality, but the difference is very small (less than 1 °C) and may not be significant. In any case, we see that, for the two days of interest, the UTCI values at night are all comprised between 9 and 26 °C, which corresponds to the "no heat stress" UTCI band. Solar radiation is an important factor for human thermal comfort. During the morning (until 10:00 UTC) the shading caused by the east wall prevents heat stress inside the street while the outside of the street is in a situation of moderate heat stress (26 °C ≤ UCTI < 32 °C): the inside of the street is actually 8.5 °C cooler in terms of UTCI than the outside of the street at 09:30 UTC. From 10:30 UTC, the position of the sun on the sunny day is such that there is no more shading in the street at human height (Figure 5) in the non-vegetated modality of the street. Consequently, the UTCI values increase abruptly (from 25 °C at 09:30 up to 34 °C at 11:00) and enter the zone corresponding to high heat stress with a peak of 36 °C at 14:00 UTC. In the vegetated street modality, the UTCI values also increase with radiation but this increase is strongly attenuated as the UTCI remains below 29.5 °C all day, keeping the street in a moderate heat stress condition at mid-day. The trees therefore reduce the UTCI by up to 8 °C at midday (between 10:30 and 14:00 UTC), reducing the heat stress category from high to moderate inside the vegetated street. From 14:00 UTC, the shading caused by the west wall reduces the heat stress felt in the street (moderate heat stress) while outside the street, the heat stress remains in a zone of high level until 17:00 UTC. For the cloudy day, there is no heat stress felt inside the vegetated street, neither during the night nor during the day. Outside the street, there is no heat stress during the night, but a moderate heat stress during the day. The UTCI is intermediate between that outside the street and in the vegetated street.

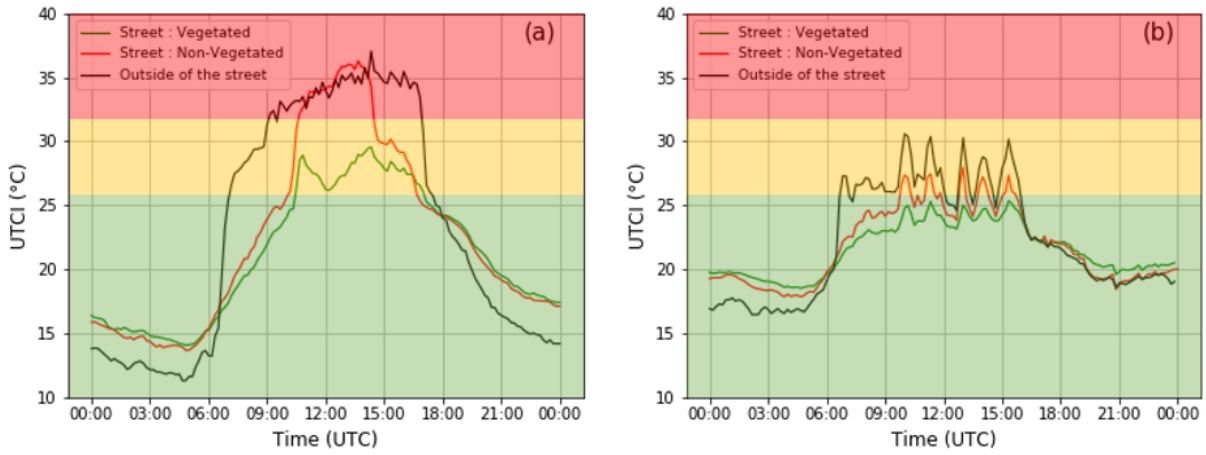

Figure 18 : Daily evolutions of UTCI outside of the street and inside the street at 0.4 m from the ground. (a): for the sunny day, (b): for the cloudy day. Red bands refer to strong heat stress (32°C ≤ UTCI < 38 °C), yellow bands refer to moderate heat stress (26 °C ≤ UCTI < 32 °C), green bands refer to no thermal stress (9 °C ≤ UTCI < 26 °C).

Concerning the impact of trees on human thermal comfort, the results shown in Figure 18 disclose trends similar to those reported in the literature (Błażejczyk et al., 2014; Cheung and Jim, 2018; Coutts et al., 2016; Redon et al., 2020). Błażejczyk et al. (2014) have shown in their study that during the summer period, the UTCI in rural areas could be up to 9.4 °C lower than the UTCI in urban areas at midnight. During daytime, they also found that in the morning and afternoon, the urban area could actually be cooler than the rural area, due to shading provided by street canyons. However, the degree of cooling in the urban area was less intense than in our study, probably due to the fact that at the city scale, streets have different orientations with different degrees of shading (while our north-south street has the shadiest orientation in summer) and the whole city has more inertia than an isolated street. Coutts et al. (2016) also estimated the UTCI in three canyon streets in Melbourne City. The east-west

orientation of their streets shows some differences in temporal evolution compared with our street, especially in the morning and afternoon when shading effects from the walls are less important than in our north-south orientated street. When averaging all measurement positions within each street, the maximum reduction values in UTCI by trees compared to areas free of trees, also obtained at midday, was between 2 and 3 °C, lowering heat stress from a very high level (UTCI > 38 °C) to a high level (38 °C > UTCI > 32 °C). For the measurement station located right under a tree crown, the reduction in UTCI could reach 7 °C, in good agreement with our results. Coutts et al. (2016) also found that, during heat events, trees in east-west oriented canyons with average aspect ratio between 0.27 and 0.76 had a low impact on air temperature (0.9 °C at mid-morning) but a significant impact on diurnal UTCI index in summer, largely due to a reduction in the mean radiant temperature, reducing heat stress from a very high level to a high level. In their study on the comparison of the cooling effects of a tree and a concrete shelter conducted in Hong Kong (22.32° N, 114.20° E), in China, during the summer period of 2017, Cheung and Jim (2018) have shown that the tree can reduce the heat stress index by up to 10.3 °C – this maximum cooling effect of the trees was also observed around midday, when the solar radiation was the strongest. Our observations on the daily evolutions of UTCI can also be compared to those obtained numerically with the TEB model by Redon et al. (2020) with similar orientation (12° angle to the north), and percentage of ground covered by trees (70 %), but with a different aspect ratio (0.55) and with bare soil under the trees (whereas in our study it is sealed asphalt soil). In Redon et al. (2020), the UTCI of the treeless canyon reaches a maximum of 35 °C with a strong heat-stress sensation at midday which is similar to our results, but the strong shadowing effect of the walls in early morning and late afternoon is not visible, due to the canyon lower aspect ratio. The trees only reduce by 3 °C the UCTI, which is lower than the reduction we obtain. This may be due to the fact that the ground under the tree in the TEB study is bare soil rather than asphalt; therefore, is has a higher albedo, and hence the benefit of the trees may not be as marked.

3.10 Energy balance in the non-vegetated modality of the canyon street

An energy balance (Eq. 13) was carried out in the non-vegetated street mode, over 24 hours during the selected sunny and cloudy days considering the volume (see Figure 5) and methods described in section 2.3.4. The sensible heat flux was deduced from radiation and conductive heat fluxes measurements. Results show that the dissipation of energy in the street modality occurs more through convection than through conduction (Table 6). Indeed, over a 24 hours period, the conductive heat flux changes sign (from positive during the day to negative during the night, see Figure 9), which can in part cancel out the cumulated value. Here, on a sunny day, only 16 % of the energy is dissipated by conduction, the remaining amount being dissipated by convection.

The daily totals of net radiation and transpiration for the three central trees of the street vegetated modality are provided in Table 7. To convert tree transpiration from L day^{-1} to MJ m^{-2} day^{-1}, we used the density of water, the latent heat of vaporization of water and a reference surface corresponding to the surface of the street occupied by the 3 central trees (see Figure 5). We estimated the reference surface of the street equal to 4.8 m^2. The corresponding values of the transpiration per m^2 are lower than those obtained in section 3.6 for which the reference area was the projected area of the crown only (1.04 m^2 per tree i.e. 3.12 m^2 for three trees). For this case, the conductive heat flux could not be calculated, as we only have fluxmeters on the vertical walls but not on the ground in this part of the street. As it can be seen, the total net radiation is larger by 34 % in the vegetated modality than in the non-vegetated one due to the absorption of solar radiation by the trees and to the presumably high albedo of the white walls. Therefore, there is less absorption of solar radiation during the morning and the afternoon in the non-vegetated modality than in the vegetated modality. In a real city, the walls, after some years, become more greyish and this may not be as marked. Transpiration accounts for 22 % of the net radiation for the sunny day and 32 % of the net radiation for the cloudy day. In the vegetated modality, the energy

dissipated by transpiration does not fully compensate the increase in net radiation. However, the excess of the energy is absorbed by the trees at crown height. The lower part of the street, at human height, benefits from the shading of the trees with a large improvement of UTCI at midday (see Figure 18).

	Net radiation (MJ m^{-2} day^{-1})	Conductive heat flux (MJ m^{-2} day^{-1})	Sensible heat flux (MJ m^{-2} day^{-1})
Sunny day	10.19	1.63	8.55
Cloudy day	3.69	-2.27	5.95

Table 6: Accumulation of the different terms of the energy balance (computed over the whole day) on the non-vegetated modality of the canyon street.

	Net radiation (MJ m^{-2} day^{-1})	Transpiration (MJ m^{-2} day^{-1})	Ratio Transpiration/Net radiation (%)
Sunny day	13.72	3.02	22
Cloudy day	4.97	1.59	32

Table 7: Accumulation of the net radiation (computed over the whole day) and of the transpiration of the three central trees in the vegetated modality of the canyon street.

4 Discussion

The present study is probably among the first to use alignment trees as a vegetation solution in a canyon street in a reduced-scale outdoor environment, hence the difficulty of being able to compare our results with those of the literature. The trends we observed on the climatic variables and impact of the vegetation are however in agreement with those identified in the synthesis of studies on the cooling effects of vegetation on the urban heat island published by Qiu et al. (2013). Their paper points out that the climatic benefits that trees can provide depend on several factors such as the scale of the study, the aspect ratio, the orientation of the street, the type of vegetation used, the rate of vegetation cover and the local climatic conditions. In the following, we will first discuss the possible influence of our experimental configuration (isolated reduced-scale street, North-South orientation, absence of human activity) on the street microclimate. Then, we will analyze and discuss the trees climatic benefits, with special emphasis on the partitioning between shading and transpiration.

4.1 Impact of the canyon street scale reduction on the energy balance

Our canyon street is an isolated canyon street, at reduced-scale (1/5), north-south oriented with white painting on the walls and an aspect ratio of 1. We will first discuss the impact of the street geometrical reduction factor on the energy balance of the street, given in Eq. 13. Provided the urban materials are the same (in terms of surface optical factor, thermal conductivity, and material thickness), and the geometrical aspect ratio of the street is conserved, then the radiation and conductive fluxes are conserved and are not directly impacted by the scale reduction.

Regarding the sensible heat flux (convective heat transfer), it can be affected by the wind speed, the temperature gradient between the surfaces and the air, and the type of convection regime (through different formulae of the convection coefficients). We have shown earlier in the results that the surface temperatures were correctly represented (given our configuration, with a north-south orientation and a light painting on the walls). As far as the wind speed is concerned, our site is quite sheltered from the wind, but so are urban spaces. Reynolds number independence is achieved thanks to the characteristic dimension of the street which remains large (H = 2 m) and ensures a flow in the fully turbulent regime. Indeed, with a wind velocity of $U = 1$ m s^{-1}, this yields a Reynolds number of $Re = UH/\nu \approx 130000$, (with ν the kinematic viscosity of air) which is largely above the critical number $Re_c = 11000$ for

atmospheric flows around sharp-edges obstacle bodies (Snyder, 1972).

The main discussion here lies on the type of convection regime. The non-dimensional number of interest here is the Richardson number (Eq. 6 in section 2.3.2), which gives the relative importance of inertial forces and buoyancy forces (due to air temperature gradient) on the flow field. Eq. 6 shows that, for the same free stream velocity and wall and free stream temperatures, the importance of the buoyancy forces will be reduced by the same factor as the geometrical scale reduction factor on the building height which here is equal to 5. Hence it can be expected that on the reduced-scale model, the thermal effects on the flow field will be reduced by 5 compared to the inertial forces. Natural convection regimes are therefore difficult to reproduce, and our facility is better suited for the investigation of flows in the forced or mixed convection regimes. Indeed, we saw here that during the investigated sunny day, the Richardson number reached a value of -4 for our experiment (Figure 6) corresponding to a mixed convection regime. In comparison, Louka et al. (2002) obtained a Richardson number of the order of -10 (in the natural convection regime) on a sunny summer day in their full-scale study in Nantes (computed here from their results of air and surface temperature, wall height and wind speed); in their reduced-scale study, Idczak et al. (2007) obtained a Richardson number of -0.9, at the beginning of the mixed convection regime (with weaker thermal effect than us, possibly owing to a higher wind speed). Hence the sensible heat flux can be affected by the above-mentioned considerations on the flow field and Richardson number, but this impact is expected to be small provided the wall temperatures are the same and the flow remains in the same type of convection regime (where the same convection coefficient formula applies). This assumption is made (explicitly or not) by most authors working on reduced-scale models (Chen et al., 2020; Djedjig et al., 2015).

Finally, regarding the latent heat flux density, corresponding to the tree transpiration, it depends on the tree species, the LAI, the street area covered by the trees, the water availability in the ground and the climatic conditions. We show below (section 4.3) that the tree LAI in our facility is representative of other urban studies at full-scale. Therefore, the latent heat flux density can be expected to be comparable to a full-scale situation in well-watered conditions, with same LAI and tree coverage area.

The benefit of working on a scale-model in outdoor environment is to mimic a canonical urban environment at a lower experimental cost, while benefiting from realistic climatic conditions (including radiation and wind). It also makes it possible to use a more extensive and dense instrumentation than in real cities.

4.2 Impact of the canyon street configuration and its environment on urban overheating

We will discuss here the impact of our experimental configuration on urban overheating, in relation with factors other than scale reduction (that we just discussed above). Compared to the outside of the street, we measured a maximum urban overheating of 2.8 °C at night and of 2.4 °C during daytime. The north-south orientation of our canyon street is the one for which the shading effects of the building walls are more important during the summer period (Andreou et al., 2014). In addition, our walls are quite reflective (white painting). Altogether, this is likely to induce moderate wall surface temperatures and hence air temperatures increase in the canyon during daytime, compared to other configurations (Doya et al., 2012; Najjar et al., 2005). At nighttime, one may question whether an isolated street may cool down more quickly than an ensemble of several neighboring streets, resulting in a lower urban overheating at night. But the comparison with the results from of the facilities of Wang et al. (2017) and Doya et al. (2012) consisting of several adjacent reduced-scale canyons, does not show any effect of the number of canyons and in fact our urban overheating at night was actually larger than theirs (see section 3.7).

Regarding the fact that our street is not in a real dense city center, it may surely affect the intensity of

measured urban overheating. First of all, inside a real city, the air temperature in a street is impacted by the air temperatures in the surrounding streets, which may have different orientations leading to different sun exposure and sheltering effect from the wind. Therefore, it is expected that the impact of the street orientation inside a full city would not be as strong as in an isolated street such as ours. In addition, over consecutive days of heat waves, the whole city having more inertia than an isolated street, the heat may accumulate more over the days. Therefore, our difference in air temperature between the inside and the outside of the canyon cannot directly be compared with the maximum urban heat island effect in real city. The air temperature difference we measured at the scale of the street corresponds to urban overheating, as defined by ADEME (French Ecological Transition Agency), while Urban Heat Island (UHI) refers to the larger city scale.

Another difference that may arise between our street configuration (as in other mock-up streets) and a real city is of course linked to the human activity and the associated anthropogenic heat, caused by industrial activity, road traffic or heat release by the buildings (due to heating or air conditioning). The amplitude of anthropogenic heat can be impacted by the population density, the climate (in connection with heating/air-conditioning demand), the building insulation, and the degree of use of air conditioning (Pigeon et al., 2007; Sailor and Lu, 2004). It has been measured on a city scale by Pigeon et al. (2007) in Toulouse, France. Toulouse is a medium size city in the south west of France with a larger population than Angers, a comparable climate (both cities have temperate climate without dry season, classified as Cf according to the Köppen-Geiger classification, but Toulouse has a 2.5 °C warmer summer) and limited domestic use of air-conditioning in summer, like the majority of French or to a larger extent of European cities. Pigeon et al. (2007) established that the anthropogenic heat flux in Toulouse was variable over the year but that it was lower in summer (of the order of 30 W m^{-2}) because the heating demand is less important during this period. In Angers, with a lower population and slightly cooler summer, the anthropogenic heat flux is expected to be even less. Besides, 30 W m^{-2} represents less than 5 % of the net radiation that we measured on our street (which is of the order of 650 W m^{-2} at 12:00 UTC). We can therefore assume that not reproducing the anthropogenic heat flux in our street did not significantly affect the results. Of course, for cities where the energetic demand is higher in summer due to a warmer climate in conjunction with a broader use of air-conditioning (or conversely in winter due to heating), neglecting the anthropogenic heat flux could be more problematic.

4.3 Climatic benefits of the trees

In our Canyon street, the ground has a vegetation cover ratio of 60 % in the vegetated modality, and the trees have a LAI of 2.49 m^2 m^{-2} and a LAD of 2.26 m^2 m^{-3}. It has been identified in Table 2 that the street vegetation cover ratio varies from one study to another from 30 to 90 %. In the study from Gebert et al. (2019), the LAI of the different trees were comprised between 1.13 and 2.36 m^2 m^{-2}, whereas in their meta-analysis on trees in urban situations Rahman et al. (2020) report average LAI of 3.19 ± 1.13 m^2 m^{-2} on the basis of 49 studies devoted to cooling by shading and 4.08 ± 1.47 m^2 m^{-2} on the basis of 23 studies devoted to cooling by transpiration. Gillner et al. (2015) got a LAD comprised between 0.9 and 2.56 m^2 m^{-3} in their study. The trees in our street thus have tree cover ratio, LAI and LAD within the range of the literature.

We have shown that in our north-south oriented canyon, the strongest impact of the central row of trees on thermal comfort occurs at midday, from 10:30 to 14:00 UTC, with a reduction up to 8 °C in UTCI. This is in good agreement with the results of Błażejczyk et al. (2014) and Coutts et al. (2016). Earlier in the morning and later in the afternoon, the orientation and aspect ratio of the street are such that the walls provide enough shading to stay in the no-heat stress comfort zone. The central row of trees, although not so commonly found in cities is therefore very adequate for north-south oriented street. At night, we found no benefit of the trees on thermal comfort.

The extensive instrumentation has allowed to quantify, from the energetics point of view, the total

benefits of the trees, and the relative part of transpiration and shading in the improvement of thermal comfort. Taking as a reference area the projected area of the tree crown, the trees allow to reduce global radiation during the sunny day by 13.34 MJ m^{-2} day^{-1} at z = H/5 (human height) through shading, while their transpiration dissipates 4.66 MJ m^{-2} day^{-1}, out of an incident global radiation of 25.5 MJ m^{-2} day^{-1} at z = H. The walls also participate in reducing by 8.18 MJ m^{-2} day^{-1} incident global radiation at the center of the street, through shading in the morning and in the afternoon. In total, between z = H and z = H/5 under their crown, the trees therefore reduce by 53 % the incoming energy flux density. Shading represents 74 % of the benefit and transpiration 26 % of the benefit. Shading is therefore almost 3 times more important than transpiration from the energetics point of view. For human thermal comfort, the impact of shading may be even more important, since heat dissipation through transpiration occurs at crown height, rather than at human height. It must also be reminded that our trees are well-watered. Therefore, under water restriction, as it frequently occurs during the summer, the benefit of tree transpiration may be less important. However, it should be reminded that tree transpiration also contributes to keep the leaves surface cool, thus preventing an excess of heat due to long-wave radiation. As a matter of fact, a study by Kántor et al. (2017) has shown that trees were more effective than sun sails in improving thermal comfort.

5 Conclusion

This work consisted in comparing the climate inside and outside a small-scale canyon street on the one hand and assessing the impact of well-watered trees on the microclimate inside the canyon street on the other hand. The results were analyzed during a sunny and a cloudy day in the summer season. Almost all the variables on which the microclimate depends as well as their spatial distributions were recorded. An originality of this study is to provide in a unique study an overview of many variables and phenomena that are often split over several studies. This makes it easier to assess their relative magnitude and will thus contribute to progress in the understanding of the urban climate as influenced by the street structure and the vegetation. In summary, the experimental results showed that, at human height (z = H/5), in the non-vegetated modality, the street and its buildings:

- intercepted 32 % of the solar incident energy on the street during the sunny day and 28 % of the solar incident energy on the cloudy day, thanks to the shading effects of the walls.
- were responsible for an urban overheating on air temperature of 2.8 °C during the night and 2.4 °C during daytime (maximum values for the sunny day), compared to the outside environment.
- generated a morning cooling of 1.2 °C on air temperature (maximum value for the sunny day) compared to outside environment, due to the shading from the east wall and to the thermal inertia of the urban materials.
- reduced the UTCI by up to 8 °C (maximum value for the sunny day) in the early morning and late afternoon thanks to the shading of the walls.

As for the trees, we observed that they:

- intercepted through their crown 53 % of the incident solar energy on the street during the sunny day and 55 % on the cloudy day.
- increased the total net radiation (measured at z = H) over a 24 hours period by 34 % (in relation with the above-mentioned interception), and dissipated about 22 % of the total net radiation through to their transpiration during the sunny day.
- diminished the air temperature at z = H/5 from the ground (equivalent to 2 m at full-scale, that is at human height) at mid-day by up to 2.7 °C during the sunny day, and by up to 1.2 °C during the cloudy day, thus cancelling out the urban overheating in the street.
- reduced the conductive heat flux on western wall by 99 W m^{-2} and by 76 W m^{-2} on the eastern wall for the sunny day.

- reduced by about 18 °C the peak of ground temperature and by about 7 °C the peak of temperatures of the eastern and western walls thanks to shading for the sunny day.
- reduced the UTCI by up to 8.0 °C (at 13:00 UTC) in the street during the day, thus reducing the heat stress from strong to moderate for the sunny day.

In spite of sometimes different areas of study or vegetalization solutions, the effects of the street and trees on the microclimate observed during the two studied days are globally of the same order of magnitude as those observed in the literature. It suggests that our reduced-scale model is able to correctly reproduce the main physical and ecophysiological processes occurring inside a street.

Regarding recommendations to urban planners, this study shows that a central row of trees, although not so commonly found in cities, is especially well adapted for North-South oriented streets with an aspect ratio of 1, which can be considered as intermediate between deep and shallow canyons. Indeed, the daily temporal evolution of UTCI values shows that, in this configuration, the street benefits from shading through the whole day: in the morning and afternoon, thanks to the building walls, and at mid-day (when the solar radiation reaches its maximum), thanks to the street trees.

Finally, in this work, we took care to maintain and check the well-watered status of the trees through the measurement of soil water potential, whereas this status is usually unknown or not reported in urban studies. In this sense, the above-mentioned climatic benefits of the urban trees should be understood as an upper limit (for our configuration), and trees in water-restriction (as it can frequently happen in summer) could provide lower benefits due to a reduced transpiration and, on the long run, a weaker development that could reduce total leaf surface area and hence shading effects. In this prospect, this work will be followed by a study of the impact of water restriction on the climatic services provided by trees within a canyon street. The use of these experimental results for the implementation of a CFD (computational Fluid Dynamics) numerical model is planned in a future publication. CFD is a numerical technique making it possible to assess the distributed climate inside the street, by solving the conservation equations for mass, momentum, and energy. Specific submodels may be also activated to solve the radiative transfers and to simulate the interactions of the trees with local climate conditions (light interception, transpiration). Once validated using experimental data, the CFD numerical model can then be used to study the influence of various parameters such as the physical properties of the materials (thermal conductivity, specific heat ...), the surface radiative properties (albedo), or the properties of the vegetation cover (leaf area, LAI ...) on the urban overheating and climatic benefits of the trees, so as to help in the decision making of urban planners. The CFD model can also be used to test a range of climatic boundary conditions such as the incident wind speed, the incident radiation (short and long wavelength), the outdoor relative humidity and the air temperature, which could be of interest in the context of climate change.

Acknowledgments

We would like to thank Dominique Lemesle (EPHor, Institut Agro) who implemented the street sensors and Patrice Cannavo (EPHor, Institut Agro) who provided his expertise on soil data analysis, Agathe Boukouya, Lydie Ledroit and Bénédicte Dubuc (IRHS, Univ Angers, Intstitut Agro, INRAE) who performed tree measurements. Our thanks also go to the staff of the Phenotic platform for their help in this project. We finally thank our tree supplier, the nurseryman Jacques Briant. This work took place within the framework of a thesis financed by Region Pays de la Loire and ADEME (French Ecological Transition Agency). It also benefited from the finiancial support of the regional program "Objectif Végétal, Recherche, Formation, et Innovation en Pays de la Loire", supported by the Pays de la Loire Region, Angers Loire Métropole and the European Regional Development Fund.

References

Aboelata, A., 2020. Vegetation in different street orientations of aspect ratio (H/W 1:1) to mitigate UHI and reduce buildings' energy in arid climate. Building and Environment 172, 106712. https://doi.org/10.1016/j.buildenv.2020.106712

Allen, R., Pereira, L., Raes, D., Smith, M., 1998. FAO Irrigation and drainage paper No. 56. Rome: Food and Agriculture Organization of the United Nations 56, 26–40.

Andreou, E., 2014. The effect of urban layout, street geometry and orientation on shading conditions in urban canyons in the Mediterranean. Renewable Energy 63, 587–596. https://doi.org/10.1016/j.renene.2013.09.051

Arnfield, A.J., 2003. Two decades of urban climate research: a review of turbulence, exchanges of energy and water, and the urban heat island. International Journal of Climatology 23, 1–26. https://doi.org/10.1002/joc.859

Athamena, K., Sini, J.-F., Rosant, J.-M., Guilhot, J., 2018. Numerical coupling model to compute the microclimate parameters inside a street canyon: Part II: Experimental validation of air temperature and airflow. Solar Energy 170, 470–485. https://doi.org/10.1016/j.solener.2018.05.015

Błażejczyk, K., Kuchcik, M., Błażejczyk, A., Milewski, P., Szmyd, J., 2014. Assessment of urban thermal stress by UTCI – experimental and modelling studies: an example from Poland. DIE ERDE – Journal of the Geographical Society of Berlin 145, 16–33. https://doi.org/10.12854/erde-145-3

Bourbia, F., Awbi, H.B., 2004. Building cluster and shading in urban canyon for hot dry climate. Renewable Energy 29, 249–262. https://doi.org/10.1016/S0960-1481(03)00170-8

Bowler, D.E., Buyung-Ali, L., Knight, T.M., Pullin, A.S., 2010. Urban greening to cool towns and cities: A systematic review of the empirical evidence. Landscape and Urban Planning 97, 147–155. https://doi.org/10.1016/j.landurbplan.2010.05.006

Bröde, P., Fiala, D., Holmér, I., Jendritzky, G., Kampmann, B., Tinz, B., Havenith, G., 2012. Deriving the operational procedure for the Universal Thermal Climate Index (UTCI). Int J Biometeorol 14.

Cannavo, P., Guénon, R., Galopin, G., Vidal-Beaudet, L., 2018. Technosols made with various urban wastes showed contrasted performance for tree development during a 3-year experiment. Environ Earth Sci 77, 650. https://doi.org/10.1007/s12665-018-7848-x

Cannavo, P., Vidal-Beaudet, L., Grosbellet, C., 2014. Prediction of long-term sustainability of constructed urban soil: impact of high amounts of organic matter on soil physical properties and water transfer. Soil Use and Management 30, 272–284. https://doi.org/10.1111/sum.12112

Cantat, O., 2004. L'îlot de chaleur urbain parisien selon les types de temps. norois 75–102. https://doi.org/10.4000/norois.1373

Chen, G., Wang, D., Wang, Q., Li, Y., Wang, X., Hang, J., Gao, P., Ou, C., Wang, K., 2020. Scaled outdoor experimental studies of urban thermal environment in street canyon models with various aspect ratios and thermal storage. Science of The Total Environment 726, 138147. https://doi.org/10.1016/j.scitotenv.2020.138147

Chen, X.-L., Zhao, H.-M., Li, P.-X., Yin, Z.-Y., 2006. Remote sensing image-based analysis of the relationship between urban heat island and land use/cover changes. Remote Sensing of Environment 104, 133–146. https://doi.org/10.1016/j.rse.2005.11.016

Cheung, P.K., Jim, C.Y., 2018. Comparing the cooling effects of a tree and a concrete shelter using PET and UTCI. Building and Environment 130, 49–61. https://doi.org/10.1016/j.buildenv.2017.12.013

Correa, E., Ruiz, M.A., Canton, A., Lesino, G., 2012. Thermal comfort in forested urban canyons of low building density. An assessment for the city of Mendoza, Argentina.

Building and Environment 58, 219–230. https://doi.org/10.1016/j.buildenv.2012.06.007
Coutts, A.M., White, E.C., Tapper, N.J., Beringer, J., Livesley, S.J., 2016. Temperature and human thermal comfort effects of street trees across three contrasting street canyon environments. Theor Appl Climatol 124, 55–68. https://doi.org/10.1007/s00704-015-1409-y
DePaul, F.T., Sheih, C.M., 1986. Measurements of wind velocities in a street canyon. Atmospheric Environment (1967) 20, 455–459. https://doi.org/10.1016/0004-6981(86)90085-5
Djedjig, R., Bozonnet, E., Belarbi, R., 2015. Experimental study of the urban microclimate mitigation potential of green roofs and green walls in street canyons. International Journal of Low-Carbon Technologies 10, 34–44. https://doi.org/10.1093/ijlct/ctt019
Doya, M., Bozonnet, E., Allard, F., 2012. Experimental measurement of cool facades' performance in a dense urban environment. Energy and Buildings 55, 42–50. https://doi.org/10.1016/j.enbuild.2011.11.001
Eliasson, I., 1996. Urban nocturnal temperatures, street geometry and land use. Atmospheric Environment, Conference on the Urban Thermal Environment Studies in Tohwa 30, 379–392. https://doi.org/10.1016/1352-2310(95)00033-X
Fiala, D., 2010. Physiological modeling for technical clinical and research applications. Front Biosci S2, 939–968. https://doi.org/10.2741/s112
Gebert, L.L., Coutts, A.M., Tapper, N.J., 2019. The influence of urban canyon microclimate and contrasting photoperiod on the physiological response of street trees and the potential benefits of water sensitive urban design. Urban Forestry & Urban Greening 40, 152–164. https://doi.org/10.1016/j.ufug.2018.07.017
Georgakis, Ch., Santamouris, M., 2006. Experimental investigation of air flow and temperature distribution in deep urban canyons for natural ventilation purposes. Energy and Buildings 38, 367–376. https://doi.org/10.1016/j.enbuild.2005.07.009
Gillner, S., Vogt, J., Tharang, A., Dettmann, S., Roloff, A., 2015. Role of street trees in mitigating effects of heat and drought at highly sealed urban sites. Landscape and Urban Planning 143, 33–42. https://doi.org/10.1016/j.landurbplan.2015.06.005
Holmer, B., Eliasson, I., 1999. Urban–rural vapour pressure differences and their role in the development of urban heat islands. International Journal of Climatology 19, 989–1009. https://doi.org/10.1002/(SICI)1097-0088(199907)19:9<989::AID-JOC410>3.0.CO;2-1
Idczak, M., Mestayer, P., Rosant, J.-M., Sini, J.-F., Violleau, M., 2007. Micrometeorological Measurements in a Street Canyon during the Joint ATREUS-PICADA Experiment. Boundary-Layer Meteorology 124, 25–41. https://doi.org/10.1007/s10546-006-9095-z
Jamei, E., Rajagopalan, P., Seyedmahmoudian, M., Jamei, Y., 2016. Review on the impact of urban geometry and pedestrian level greening on outdoor thermal comfort. Renewable and Sustainable Energy Reviews 54, 1002–1017. https://doi.org/10.1016/j.rser.2015.10.104
Kántor, N., Gulyás, Á., Gal, C., 2017. Relevance of urban trees and sun shades regarding summertime heat stress reduction – a field surveys from Pécs, Hungary. University of Szeged, Department of Climatology and Landscape Ecology, Szeged, 6722.
Kastendeuch, P., Najjar, G., Ringenbach, N., 2006. Modélisation du bilan radiatif et d'énergie d'un canyon urbain à Strasbourg. Climatologie. https://doi.org/10.4267/climatologie.677
Kuddus, M.A., Rahman, A., 2015. Affect of Urbanization on Health and Nutrition. International Journal of Statistics and Systems 10, 165–175.
Lauzet, N., 2019. Prise en compte cumulée du réchauffement climatique et des surchauffes

urbaines en phase amont de conception frugale des bâtiments centrée sur le confort des occupants : des propositions méthodologiques (phd). Lorient.
Lemonsu, A., Grimmond, C.S.B., Masson, V., 2004. Modeling the Surface Energy Balance of the Core of an Old Mediterranean City: Marseille. Journal of Applied Meteorology 43, 16.
Liang, W., Huang, J., Jones, P., Wang, Q., Hang, J., 2018. A zonal model for assessing street canyon air temperature of high-density cities. Building and Environment 132, 160–169. https://doi.org/10.1016/j.buildenv.2018.01.035
Louka, P., Vachon, G., Sini, J.-F., Mestayer, P.G., Rosant, J.-M., 2002. Thermal Effects on the Airflow in a Street Canyon – Nantes'99 Experimental Results and Model Simulations. Water, Air, & Soil Pollution: Focus 2, 351–364. https://doi.org/10.1023/A:1021355906101
Najjar, G., Kastendeuch, P.P., Ringenbach, N., Colin, J.R., Stoll, M.P., Nerry, F., Bernard, J., Hatten, A.D., Luhahe, R., Viville, D., 2005. Bilans radiatif et d'énergie dans un canyon urbain. Climatologie 41–57.
Nakamura, Y., Oke, T.R., 1988. Wind, temperature and stability conditions in an east-west oriented urban canyon. Atmospheric Environment (1967) 22, 2691–2700.
Niachou, K., Livada, I., Santamouris, M., 2008. Experimental study of temperature and airflow distribution inside an urban street canyon during hot summer weather conditions. Part II: Airflow analysis. Building and Environment 43, 1393–1403. https://doi.org/10.1016/j.buildenv.2007.01.040
Oke, T.R., Maxwell, G.B., 1975. Urban heat island dynamics in Montreal and Vancouver. Atmospheric Environment (1967) 9, 191–200. https://doi.org/10.1016/0004-6981(75)90067-0
Ouldboukhitine, S.-E., Belarbi, R., Jaffal, I., Trabelsi, A., 2011. Assessment of green roof thermal behavior: A coupled heat and mass transfer model. Building and Environment 46, 2624–2631. https://doi.org/10.1016/j.buildenv.2011.06.021
Park, M., Hagishima, A., Tanimoto, J., Narita, K., 2012. Effect of urban vegetation on outdoor thermal environment: Field measurement at a scale model site. Building and Environment 56, 38–46. https://doi.org/10.1016/j.buildenv.2012.02.015
Pigeon, G., Legain, D., Durand, P., Masson, V., 2007. Anthropogenic heat release in an old European agglomeration (Toulouse, France). Int. J. Climatol. 27, 1969–1981. https://doi.org/10.1002/joc.1530
Qiu, G., Li, H., Zhang, Q., Chen, W., Liang, X., Li, X., 2013. Effects of Evapotranspiration on Mitigation of Urban Temperature by Vegetation and Urban Agriculture. Journal of Integrative Agriculture 12, 1307–1315. https://doi.org/10.1016/S2095-3119(13)60543-2
Rahman, M.A., Stratopoulos, L.M.F., Moser-Reischl, A., Zölch, T., Häberle, K.-H., Rötzer, T., Pretzsch, H., Pauleit, S., 2020. Traits of trees for cooling urban heat islands: A meta-analysis. Building and Environment 170, 106606. https://doi.org/10.1016/j.buildenv.2019.106606
Redon, E., 2017. Modélisation de la végétation urbaine comme régulateur thermique (phd). Université de Toulouse, Université Toulouse III - Paul Sabatier.
Redon, E., Lemonsu, A., Masson, V., 2020. An urban trees parameterization for modeling microclimatic variables and thermal comfort conditions at street level with the Town Energy Balance model (TEB-SURFEX v8.0). Geoscientific Model Development 13, 385–399. https://doi.org/10.5194/gmd-13-385-2020
Ridha, S., 2017. Urban heat Island mitigation strategies in an arid climate. In outdoor thermal comfort reacheable (phd). INSA de Toulouse.

Rizwan, A.M., Dennis, L.Y.C., Liu, C., 2008. A review on the generation, determination and mitigation of Urban Heat Island. Journal of Environmental Sciences 20, 120–128. https://doi.org/10.1016/S1001-0742(08)60019-4

Rotach, M.W., 1995. Profiles of turbulence statistics in and above an urban street canyon. Atmospheric Environment 29, 1473–1486. https://doi.org/10.1016/1352-2310(95)00084-C

Rotach, M.W., Vogt, R., Bernhofer, C., Batchvarova, E., Christen, A., Clappier, A., Feddersen, B., Gryning, S.-E., Martucci, G., Mayer, H., Mitev, V., Oke, T.R., Parlow, E., Richner, H., Roth, M., Roulet, Y.-A., Ruffieux, D., Salmond, J.A., Schatzmann, M., Voogt, J.A., 2005. BUBBLE – an Urban Boundary Layer Meteorology Project. Theoretical and Applied Climatology 81, 231–261. https://doi.org/10.1007/s00704-004-0117-9

Sailor, D.J., Lu, L., 2004. A top–down methodology for developing diurnal and seasonal anthropogenic heating profiles for urban areas. Atmospheric Environment 38, 2737–2748. https://doi.org/10.1016/j.atmosenv.2004.01.034

Santamouris, M., Papanikolaou, N., Koronakis, I., Livada, I., Asimakopoulos, D., 1999. Thermal and air flow characteristics in a deep pedestrian canyon under hot weather conditions. Atmospheric Environment 33, 4503–4521. https://doi.org/10.1016/S1352-2310(99)00187-9

Santamouris, M., Papanikolaou, N., Livada, I., Koronakis, I., Georgakis, C., Argiriou, A., Assimakopoulos, D.N., 2001. On the impact of urban climate on the energy consumption of buildings. Solar Energy 70, 201–216. https://doi.org/10.1016/S0038-092X(00)00095-5

Shashua-Bar, L., Hoffman, M.E., 2003. Geometry and orientation aspects in passive cooling of canyon streets with trees. Energy and Buildings 35, 61–68. https://doi.org/10.1016/S0378-7788(02)00080-4

Snyder, W.H., 1972. Similarity criteria for the application of fluid models to the study of air pollution meteorology. Boundary-Layer Meteorol 3, 113–134. https://doi.org/10.1007/BF00769111

Susca, T., Gaffin, S.R., Dell'Osso, G.R., 2011. Positive effects of vegetation: Urban heat island and green roofs. Environmental Pollution 159, 2119–2126. https://doi.org/10.1016/j.envpol.2011.03.007

Tapper, N.J., 1990. Urban influences on boundary layer temperature and humidity: Results from Christchurch, New Zealand. Atmospheric Environment. Part B. Urban Atmosphere 24, 19–27. https://doi.org/10.1016/0957-1272(90)90005-F

United Nations, 2018. Word Urbanization Prospects : The 2018 Revision.

Vailshery, L.S., Jaganmohan, M., Nagendra, H., 2013. Effect of street trees on microclimate and air pollution in a tropical city. Urban Forestry & Urban Greening 12, 408–415. https://doi.org/10.1016/j.ufug.2013.03.002

Vidal-Beaudet, L., Grosbellet, C., Forget-Caubel, V., Charpentier, S., 2012. Modelling long-term carbon dynamics in soils reconstituted with large quantities of organic matter. European Journal of Soil Science 63, 787–797. https://doi.org/10.1111/j.1365-2389.2012.01494.x

Wang, Q., Li, Y., Hang, J., Peng, L., 2017. The Diurnal Cycle of Urban Thermal Environment in Scale-model Street Canyons by Outdoor Field Measurement. Procedia Engineering, Urban Transitions Conference, Shanghai, September 2016 198, 743–757. https://doi.org/10.1016/j.proeng.2017.07.126

Weng, Q., Lu, D., Schubring, J., 2004. Estimation of land surface temperature–vegetation abundance relationship for urban heat island studies. Remote Sensing of Environment 89, 467–483. https://doi.org/10.1016/j.rse.2003.11.005

WUCOLS, 2000. Estimating Irrigation Water Needs of Landscape Plantings in California,

University of California Cooperative extension and California Department of Water ressources, 160p.
Xiong, Y., Huang, S., Chen, F., Ye, H., Wang, C., Zhu, C., 2012. The Impacts of Rapid Urbanization on the Thermal Environment: A Remote Sensing Study of Guangzhou, South China. Remote Sensing 4, 2033–2056. https://doi.org/10.3390/rs4072033
Yang, L., Qian, F., Song, D.-X., Zheng, K.-J., 2016. Research on Urban Heat-Island Effect. Procedia Engineering 169, 11–18. https://doi.org/10.1016/j.proeng.2016.10.002

Table des matières